JACS
JOURNAL OF THE AMERICAN CHEMICAL SOCIETY

ARTICLE

pubs.acs.org/JACS

Molecular Structure Encodes Nanoscale Assemblies: Understanding Driving Forces in Electrostatic Self-Assembly

Immanuel Willerich and Franziska Gröhn*

Department of Chemistry and Pharmacy and Interdisciplinary Center for Molecular Materials, Friedrich-Alexander-University Erlangen-Nürnberg, Egerlandstraße 3, 91058 Erlangen, Germany

ABSTRACT: Supramolecular nanoparticles represent a key field in recent research as their synthesis through self-assembly is straightforward and they often can respond to external triggers. A fundamental understanding of structure-directing factors is highly desirable for a targeted structure design. This contribution demonstrates a quantitative relation between the size of supramolecular self-assembled nanoparticles and the free energy of association. Nanoparticles are prepared by electrostatic self-assembly of cationic polyelectrolyte dendrimers as model macroions and oppositely charged di- and trivalent organic dye molecules relying on the combination of electrostatic and $\pi-\pi$-interactions. A systematic set of sulfonate-group carrying azo-dyes was synthesized. Light scattering and ζ-potential measurements on the resulting nanoparticles yield hydrodynamic radii between 20 nm < R_H < 50 nm and positive ζ-potential values indicating a positive particle charge. Studies on dye self-aggregation and dendrimer-dye association by isothermal titration calorimetry (ITC) and UV−vis spectroscopy allow for the correlation of the thermodynamic parameters of dendrimer-dye association with the size of the particles, showing that at least a free energy gain of $\Delta G \approx -32$ kJ mol^{-1} is necessary to induce dendrimer interconnection. Structural features of the azo dyes causing these to favor or prevent nanoparticle formation have been identified. The dye−dye-interaction was found to be the key factor in particle size control. A simple model yields a quantitative relation between the free energy and the particle sizes, allowing for predicting the latter based on thermodynamic measurements. Hence, a set of different molecular "building bricks" can be defined where the choice of building block determines the resulting assembly size.

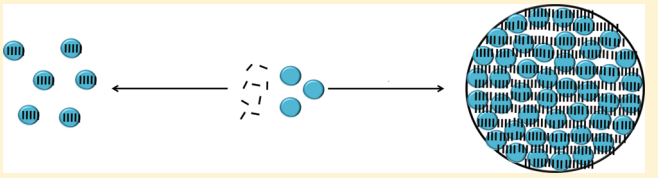

1. INTRODUCTION

Understanding structure-directing factors in self-assembly systems yielding nanostructures with defined size is of interest for fundamental and practical reasons, as it allows for a rational design of supramolecular assemblies like responsive nanostructures,[1−9] supramolecular polymers,[10−13] composite materials,[14−19] or carrier systems.[20−27] Consequently, discovering common underlying principles of structure formation in such systems is highly desirable. In multiple cases, the structure of the building blocks has been identified as a key feature with regard to the final assembly structure.[28−31] Currently, understanding self-assembled structures is in focus of theoretical studies by molecular dynamics or analytical theory development to gain insights into driving forces and basic principles.[32−35] Of interest are, for example, naturally occurring systems where understanding of the fundamental principles allows for a rational design of synthetic equivalents, e.g., the discovery of structure−property relations in biological photosystems allowed their artificial mimicking for light-harvesting applications.[36−40]

Recently, we introduced a new pathway toward nanoparticles through electrostatic self-assembly of macroions and organic counterions.[9,41−48] It represents a facile route to supramolecular assemblies in solution where well-defined spherical, rod-like or hollow sphere structures with narrow size-distribution can be created by simple mixing of the building blocks. It was shown that azo dye building blocks interconnect dendrimeric macroions into nanoparticles with sizes larger than 10-fold the initial size.[26,49,50] Thus, different from well-known and versatile host−guest complexes consisting of individual loaded host molecules,[51−53] the self-assembly process here proceeds to a second hierarchical level of interconnected host molecule structures. Those particles can respond to external triggers like pH or light with reversible dis- and reassembly or precisely controllable particle size changes.[8,54−56] This may be of particular interest for electrostatically assembled vesicles as smart carrier system or polyelectrolyte- porphyrin assemblies as functional nanosystems.[26,56] Furthermore, the structure formation does not rely on specifically synthesized binding motifs but rather on a combination of electrostatic interaction and short-range geometric effects and/or $\pi-\pi$-stacking.

While responsiveness and structural versatility were demonstrated, and recently the influence of the dendrimer building block size, i.e., the dendrimer generation, was quantitatively studied,[57] fundamental and systematic understanding on how the molecular structure of the organic counterions relates to assembly features is lacking. The objective of this work is to establish a quantitative relation between the molecular counterion structure, the ability of the counterions to interconnect the polyelectrolyte molecules, and the resulting assembly sizes, with the goal to develop a box of molecular "building bricks" allowing

Received: August 11, 2011
Published: November 03, 2011

Scheme 1. Azo Dye and Dendrimer Building Blocks

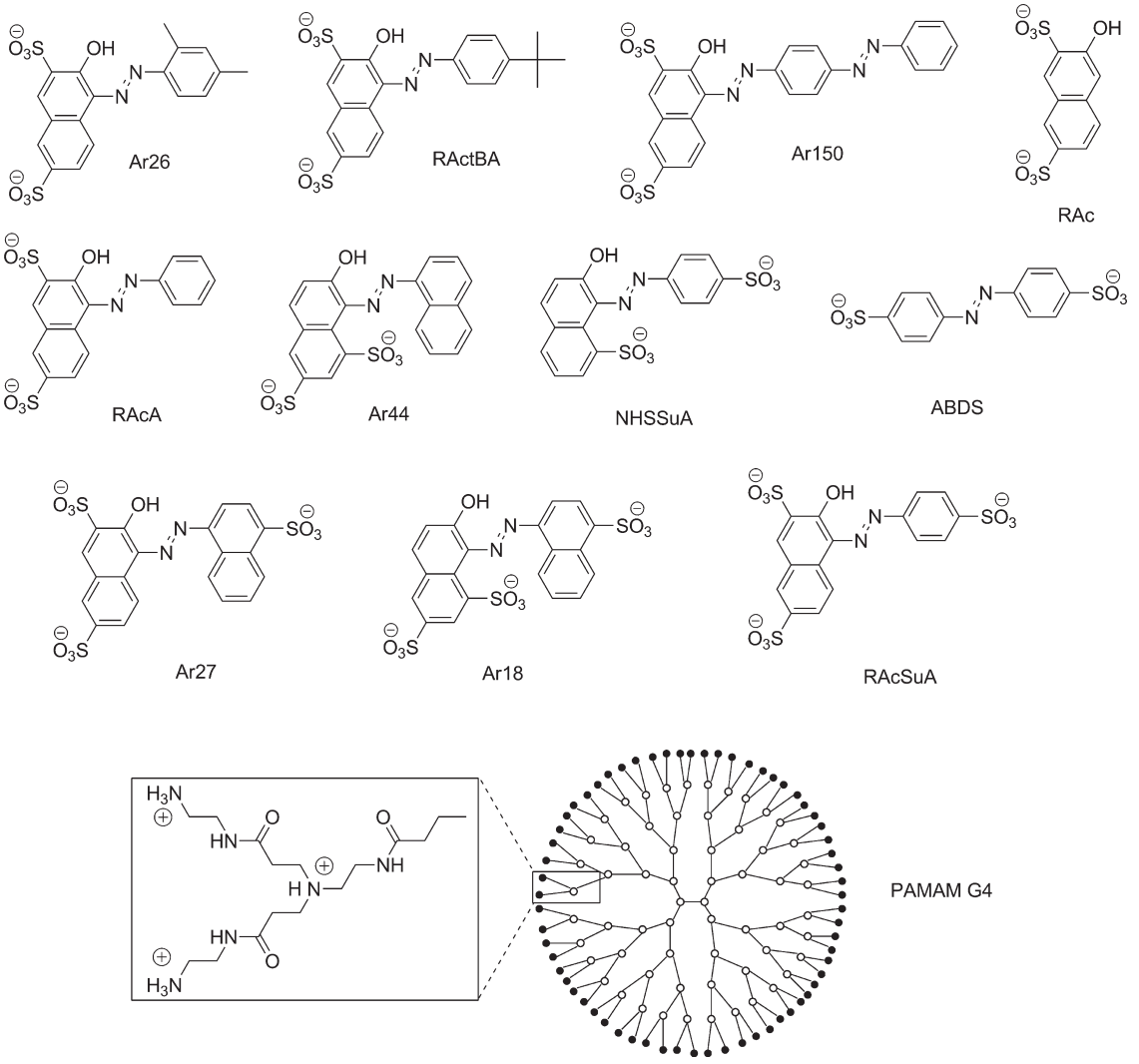

for a targeted structural design. In the present study, we investigate electrostatically self-assembled nanoparticles from polyamidoamine (PAMAM) dendrimers and oppositely charged azo dyes. For this purpose, a set of azo-dyes with the same aromatic backbone but different substituents was synthesized. To gain insight into the impact of the molecular dye structure on the assembly formation, we investigate a large set of dyes combined with generation four PAMAM dendrimer in terms of structure and thermodynamics. We present quantitative results on the delicate balance of the factors governing structure formation. One important task is to elucidate the conditions under which an azo dye is able to interconnect dendrimer molecules into nanoparticles rather than forming host−guest complexes. This may allow one, in the future, to choose a dye yielding an assembly with a desired size, stability, and functionality.

2. RESULTS AND DISCUSSION

Studies on assemblies from generation 4 PAMAM dendrimer and a set of azo dyes comprise structural characterization, thermodynamic analysis, and development of a simple model. Scheme 1 depicts building blocks used, some of which were previously investigated (Ar26, Ar27, Ar18, and Ar44),[49,50] while others have been specially synthesized for this study (RAcA, RActBA, RAcSuA, NHSSuA). Predominantly divalent azo dyes were chosen. Structural characterization is presented in Section 2.1, consisting of light scattering for the size analysis and ζ-potential to characterize the charge being the primary source of assembly stability. The loading ratio as the most important parameter controlling assembly formation besides building block choice is defined as the molar ratio of dye sulfonate to dendrimer primary amino groups ($l = c(SO_3^-)/c(NH_2)$). Together with the pH dependent dendrimer protonation it yields the charge ratio. In Section 2.2, a detailed analysis of assembly formation thermodynamics yields further insight and Section 2.3 focuses on a quantitative understanding of the association behavior considering the free energy in conjunction with the aggregation number.

2.1. Size and Charge Characterization. This section lays the foundation for acquiring knowledge on quantitative relations between structure and thermodynamics. To achieve this objective, it is first required to characterize the ability of different azo-dyes to form assemblies of interconnected G4 dendrimer molecules. A slight excess of 10% dendrimer charges and thus a loading ratio of $l = 1.8$ at pH = 3.5 was chosen to prepare

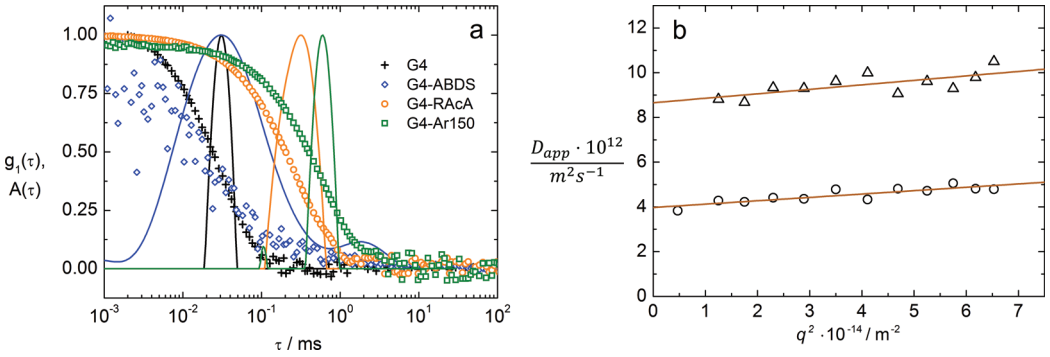

Figure 1. Dynamic light scattering data (a) Electric field autocorrelation function $g^1(\tau)$ and relaxation time distribution $A(\tau)$ of G4 dendrimer and assemblies with ABDS, RAcA, and Ar150 at a scattering angle of $\theta = 90°$; (b) extrapolation of apparent diffusion coefficients D_{app} to zero scattering angle for Ar150 (circles) and RAcA (triangles).

Table 1. Light Scattering Data for Dendrimer-Dye Samples (l = 1.8; pH = 3.5)

dye	R_H (nm)	σ	N_{Den}	R_G (nm)	R_G/R_H	I_{rel} (a.u.)
pure G4	2.3					
RActBa	38 ± 3.1	0.22 ± 0.07	2539	46 ± 3.3	1.20	(2.1 ± 1.4).10^{-3}
Ar150	48 ± 5.0	0.22 ± 0.10	5069	56 ± 5.5	1.16	(6.9 ± 1.1).10^{-3}
RAcA	24 ± 1.3	0.36 ± 0.15	630	26 ± 4.9	1.08	(6.0 ± 2.0).10^{-4}
RAc	unchanged[60]		1			
ABDS	unchanged[60]		1			
NHSSuA	unchanged[60]		1			
Ar26	43 ± 5.9	0.15 ± 0.05	3622	52 ± 7.9	1.19	(5.7 ± 2.9).10^{-3}
Ar44	22 ± 2.0	0.16 ± 0.07	478	24 ± 3.0	1.10	(6.9 ± 1.7).10^{-4}
RAcSuA	25 ± 3.7	0.21 ± 0.05	670	25 ± 9.8	1.02	(7.3 ± 5.2).10^{-4}
Ar27	33 ± 5.5	0.22 ± 0.08	1564	34 ± 6.2	1.03	(3.3 ± 1.7).10^{-3}
Ar18	23 ± 2.8	0.18 ± 0.13	569	23 ± 4.5	0.99	(5.3 ± 5.0).10^{-4}

dendrimer-dye nanoparticles, as this resulted in well-defined assemblies previously.[50] Hydrodynamic radii, radii of gyration, and scattering intensities were measured by light scattering.

First, dynamic light scattering (DLS) for G4 dendrimer in combination with three dyes, ABDS, RAcA, and Ar150 (Scheme 1) is performed to study how the molecular dye structure influences the assembly formation ability. Those dyes are chosen as they all carry two charges but differ in molecular structure. ABDS is the smallest π-conjugated system possible for an azo-dye, i.e., consists only of two benzene sulfonic acid moieties and no further substituents. The molecule in its trans-state is fully symmetric resulting in a low dipole moment. Oppositely, RAcA consists of a naphthalene moiety carrying both sulfonic groups in addition to a hydroxyl group linked to a benzene residue. Ar150 is similar to RAcA but has a larger electron system due to an additional azobenzene moiety. Figure 1a depicts the electric field autocorrelation functions $g^1(\tau)$ and the relaxation time distributions $A(\tau)$ of assemblies formed from G4 dendrimer with these azo-dyes. For ABDS, it is evident that the maximum of the relaxation time distribution does not shift to a higher value as compared to a solution of PAMAM dendrimer only. As the relaxation time corresponds to the particle radius, this indicates that this dye is not able to interconnect multiple dendrimer molecules into larger assemblies. The statistics for ABDS-G4 dendrimer samples is poor, since the scattering intensity of a diluted G4 dendrimer solution is low at the standard concentration of c = 0.044 g L^{-1} used in this study. Data for pure G4 is taken at 1 g L^{-1}. As evident from Figure 1a, RAcA in contrast shows a clear shift of the relaxation time distribution toward higher relaxation times and therefore larger particle radii. This corresponds to the fact that dye molecules interconnect the dendrimer molecules into larger supramolecular assemblies rather than just forming host−guest complexes as found for ABDS. Size-distributions are quite narrow and autocorrelation functions monomodal except for a small satellite peak at small relaxation times, which may represent an internal mode or a small amount of residual individual dendrimers. To determine accurate values for the hydrodynamic radius, the apparent diffusion coefficient D_{app} is extrapolated to zero scattering vector square (scattering angle), as shown in Figure 1b. The extrapolated diffusion coefficient can be transformed into the hydrodynamic radius R_H through the Stokes−Einstein relationship and is given in Table 1. The hydrodynamic radius for RAcA is R_H = 24 nm. When Ar150 is combined with the dendrimer, the size change is even more expressed (R_H = 48 nm). Thus one can conclude already at this point that the aromatic backbone structure of divalent azo dyes determines whether a particular dye can interconnect the dendrimers into larger structures at all and what particle size results.

Table 1 summarizes light scattering results for assemblies with dyes investigated in this study. All samples were prepared at the same dendrimer concentration of c = 0.044 g L^{-1}. For 10-fold higher or half this concentration the same trend is observed. Hydrodynamic radii for dendrimer-dye samples with loading ratios of l = 1.8 range between R_H = 20 nm and R_H = 50 nm as

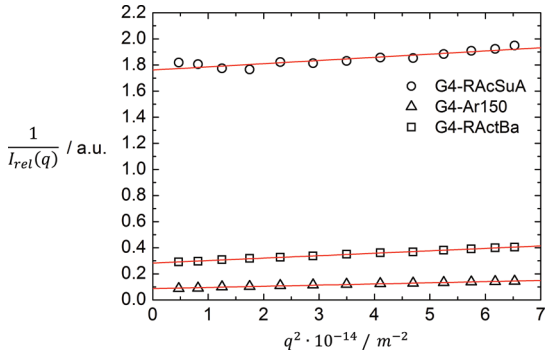

Figure 2. Static light scattering data: inverse relative intensity $1/I_{rel}$ versus scattering vector square q^2 for three selected dendrimer-dye samples.

compared to the dendrimer building block size of R_H = 2.3 nm. Interestingly, trivalent dyes do not form larger assemblies than their divalent counterparts with the same backbone. For example, RAcA and RAcSuA have the same aromatic backbone and yield almost identical R_H and scattering intensity, showing that additional charges are less effective in producing particles with larger sizes than more extended π-systems or alkyl substituents. Assemblies are stable in solution for several months. None of the dyes yielded assemblies between R_H = 2.3 nm and R_H = 20 nm, which will be discussed below. Table 1 also shows that size distributions for all dyes are narrow (standard deviation of the size distribution $0.15 \leq \sigma \leq 0.22$) with respect to other ionically self-assembled systems.[58] RAcA represents an exception and is the only dye with a significantly broader distribution (σ = 0.36). This may be due to the lack of substituents on the benzene moiety, suggesting that these have significant influence on the width of the assembly size distribution.

Figure 2 shows static light scattering results in a Zimm-type plot of inverse scattering intensity versus scattering vector square, which exhibits the typical linear relationship; i.e., no complex long-range interaction of charged species complicates the analysis and it is possible to determine the radius of gyration R_G, which is also included in Table 1. The trend corresponds to the dependence of hydrodynamic radius on molecular structure. Further, the scattering intensity extrapolated to zero scattering vector is also given in Table 1. It increases as R_H and R_G, which in combination reveals that not only the hydrodynamic dimension but also the aggregation number increases. Quantitatively, the scattering intensity for nanoparticles of different dye counterions scales approximately with $(R_{H,dye1}/R_{H,dye2})^3$. This is expected if a similar density, characteristic scattering power and particle shape is given for the different assemblies. Table 1 in addition includes the characteristic ratio R_G/R_H known to be an indication of particle shape. It lies between 1.0 and 1.2, indicating nonspherical somewhat anisotropic structures as discussed previously for some of the dyes.[43,49] As R_G/R_H does not vary too dramatically between the different samples, it is possible to estimate approximate aggregation numbers directly from the R_H. Assuming that the particle volume is given by the sum of the individual dendrimer volumes and a space of 1 nm width in between filled with dye counterions, the aggregation number N_{Den} can be approximated if the particle volume is assumed to be proportional to R_H^3. The hydrodynamic radii of the assemblies $R_{H\text{-}ass}$ and the building block $R_{H\text{-}den}$ yield $N_{Den} = (R_{H\text{-}assem}/R_{H\text{-}den})^3$. The applicability of this procedure is confirmed by the static light scattering results; that is, relative aggregation numbers extracted from the scattering intensity at zero angle—which is proportional to the molar mass and hence the aggregation number—are in agreement with the dynamic light scattering results.[59] However, this calculation should be taken as estimation rather than a quantitative result. Resulting aggregation numbers are between $N_{Den} \approx 500$ and $N_{Den} \approx 5000$ dendrimer molecules per supramolecular particle.

The dyes ABDS, RAc, and NHSSuA do not interconnect the dendrimer molecules, i.e., no size change with respect to the building block size occurs (N_{Den} = 1). Those three dyes have in common that the charged groups are not located at one side of the molecule and thus are not spatially separated from a hydrophobic moiety as for the other divalent dyes. However, if the concentration of dendrimer is gradually increased up to the factor 50, dendrimer interconnection occurs at c_{Den} = 2.87 g L^{-1} for dendrimer-ABDS samples. Nevertheless, the particles formed at this concentration are unstable in aqueous solution, grow rapidly and precipitate after few hours. For NHSSuA and RAc unstable assemblies are also observed at high concentrations. This shows that above a certain concentration threshold, aggregation can occur even for this class of dyes, but no stable assemblies are obtained. For all dyes where stable and defined assemblies can be observed at low concentration, e. g., Ar26, assembly stability does not depend on the absolute concentration until a critical salt concentration of about 30 mmolL^{-1} is exceeded, which leads to precipitation ("salting out").[49] Thus, the formation of large and unstable assemblies at high concentration for the dyes ABDS, RAc, and NHSSuA may be a salt effect, as the host−guest-complexes are salted out due to lack of electrostatic stabilization. There is no concentration for ABDS, RAc, and NHSSuA where stable assemblies form and thus these dyes are not appropriate for the goal to create supramolecular nanoparticles through electrostatic self-assembly. Consequently, this proves that the formation of well-defined and stable assemblies requires certain dye properties.

Conclusions from the size analysis are that some azo dyes are capable of interconnecting up to about 5000 dendrimer molecules into supramolecular nanoparticles, whereas for other dyes, no interconnection into stable assemblies was observed. This is in accordance to the differences in molecular dye structure. Likely differences in dye−dye-interactions are the origin as will be investigated in the following sections. For dyes capable of interconnecting dendrimers, hydrodynamic radii lie in the range of R_H = 20−50 nm with size distributions being narrow. For divalent dyes, large assemblies are favored if dye molecules contain spatially separated hydrophobic and hydrophilic aromatic moieties with alkyl-substitution or large π-electron systems as RActBa, Ar26, or Ar150. Trivalent dyes are able to interconnect the dendrimers but do not yield larger assembly sizes than their divalent counterparts.

As assembly formation is driven by the opposite charges of the building blocks and residual charge of the assembly is the origin of stability of the supramolecular particles in solution, ζ-potential measurements are a source for further insight. For assemblies with all dyes of this study, values between +44 mV < ζ < +67 mV were found, revealing that there are no expressed differences in charge density. The pure G4 PAMAM dendrimer has a ζ-potential of ζ = +88 mV showing that the charge density for the assemblies is lower than for the pure polyelectrolyte building block.[61] This is reasonable as most of the positive charges are neutralized by ion-pairing of dendrimer amino and dye sulfonate groups. Similar ζ-potential values indicate that the charge density of the assemblies is similar.[61] Thus, the limiting factor for particle growth is the

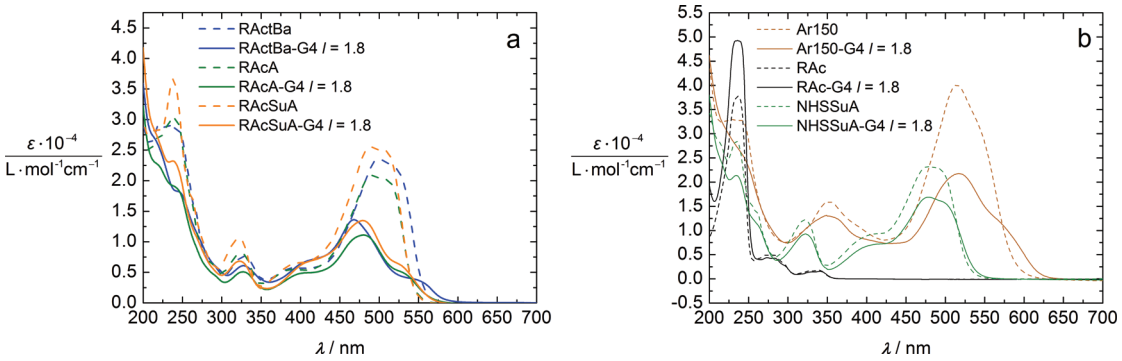

Figure 3. UV−vis spectra of azo dyes and dendrimer-dye assemblies with loading ratio l = 1.8: (a) RActBa, RAcA, and RAcSuA; (b) Ar150, RAc, and NHSSuA.

accumulation of charge as the dendrimer charges are not fully neutralized and the charge accumulated increases with increasing aggregation number.

2.2. Thermodynamic Analysis. As the structural analysis revealed distinct sizes for dyes capable of forming stable supramolecular dendrimer-dye particles, a thermodynamic analysis is highly promising to develop quantitative understanding. First, UV−vis spectroscopy is useful to analyze the binding of dendrimer and dye. The extent of band splitting, hyper- or hypsochromicity and shift of the absorption maxima indicate the strength of dye−dye-interactions.[62−64] Dye−dye interactions are induced when the dyes bind electrostatically to the dendrimer, which occurs preferably adjacently, i.e., in a cooperative process.[49]

Figure 3 shows UV−vis spectra of dye solutions and dendrimer-dye-assemblies. As evident in Figure 3a, RAcA, RActBa, and RAcSuA show comparable spectral changes upon dendrimer addition: strong hypsochromic effects, band splitting of the main band and a shift of the absorption maximum to lower wavelengths. The similar behavior of these dyes is understandable because the backbone of these three azo-dyes consists of naphthalene and benzene moieties. Very interesting is the fact that NHSSuA has the same backbone as these dyes but shows a different behavior as shown in Figure 3b: Only moderate hypsochromicity, no shift in the absorption maximum and no band splitting occurs. This indicates substantially weaker dye−dye-interactions than for the other three dyes, which is consistent with NHSSuA not being able to interconnect the dendrimer molecules into nanoparticles as opposed to RActBa, RAcA, and RAcSuA. Further, Ar150 (also included in Figure 2b) does not show a shift in the absorption maximum, but strong hypsochromicity and band splitting, which also corresponds to the large assemblies formed with this dye. RAc does not show expressed differences in its band between λ = 265 and λ = 360 nm. This may be as interactions are weak, which is consistent with the fact that the dye cannot interconnect the dendrimers. Naphthalene however is a comparably small π-electron system which does not show strong spectral shifts in general even for naphthalene dicarboxylic acids combined with PAMAM dendrimers in methanol.[42]

In conclusion, all dyes showing strong spectral changes are able to interconnect dendrimers instead of forming host−guest complexes, whereas the opposite is the case for dyes showing weak spectral changes. As discussed above, this may not be a general rule, but it is a valuable first test.

Isothermal titration calorimetry (ITC) is a powerful tool for the investigation of dendrimer-dye assembly formation as it can be used to quantify the interaction energy between dendrimer and dye by titrating the dendrimer into the dye. This "reverse procedure" is chosen as the usual titration of the ligand into the macromolecule solution is unsuitable due to the self-aggregation of the dye and wall adsorption effects.[49] In addition, the self-aggregation process of a particular dye can be investigated by dilution experiments, a procedure that may be applicable to other self-assembling systems directed by multiple interactions. Dilution experiments, where the dye is in the syringe and diluted into pure buffer in the titration cell, are useful to determine whether and to which extent a dye self-aggregates yielding self-aggregation enthalpy $\Delta H_{\mathrm{dye-dye}}$ and self-aggregation equilibrium constant $K_{\mathrm{dye-dye}}$. Further, dendrimer titration into dye solution allows for the determination of the dendrimer-dye interaction parameters $\Delta H_{\mathrm{dendr\text{-}dye}}$, $K_{\mathrm{dendr\text{-}dye}}$, and the stoichiometry parameter N_{dye}. Figure 4, Figure 5 and Figure 6 depict ITC raw data and data analysis. In the upper part of each diagram, the raw heat traces of the titration experiments are shown. For the dilution experiment, the lower part shows the integrated heat for each injection plotted versus the dye concentration in the titration cell, and the fit of the integrated heat per injection q_i according to a stepwise disaggregation model described in eqs 1 and 2. This model is mathematically identical with the previously used dimer dissociation model except that the self-aggregation enthalpy is determined per dye and not per dimer:[49,65−67]

$$q_i = \Delta H_{\mathrm{dye-dye}}\left(n_i f_{\mathrm{Agg},\,i} - n_{i-1} f_{\mathrm{Agg},\,(i-1)} - n_{\mathrm{inj}} f_{\mathrm{Agg,\,inj}}\right) \quad (1)$$

$$f_{\mathrm{Agg}} = 1 - \frac{\sqrt{(1 + 8K_{\mathrm{dye-dye}}c)} - 1}{4K_{\mathrm{dye-dye}}c} \quad (2)$$

n_i, $n_{i\text{-}1}$, and n_{inj} are the number of dye molecules in the titration cell after injection i, $i-1$ or in the syringe from which the dye solution is injected. f_{Agg} is the fraction of aggregated dye molecules and c is the dye concentration in the syringe. For the dendrimer-dye-experiments, the lower part of the figures depicts the integrated heat normalized per mole of injectant versus the molar ratio of dendrimer to dye in the titration cell. Data are fitted by the one-site model implemented in the MicroCal software.[68] The one-site model is usually used to describe independent and noninteracting binding sites. It turned out that this model describes all dendrimer-dye titrations very well, even though the binding of the dye to the polyelectrolyte is cooperative.[49,69,70] For cooperative binding of dyes to polymers an isodesmic model, i.e., the independent treatment of the binding sites, can be used if the fit is of reasonable quality. That is, it yields binding constants close to the cooperative binding constant.[49,71]

dx.doi.org/10.1021/ja207565m |J. Am. Chem. Soc. 2011, 133, 20341–20356

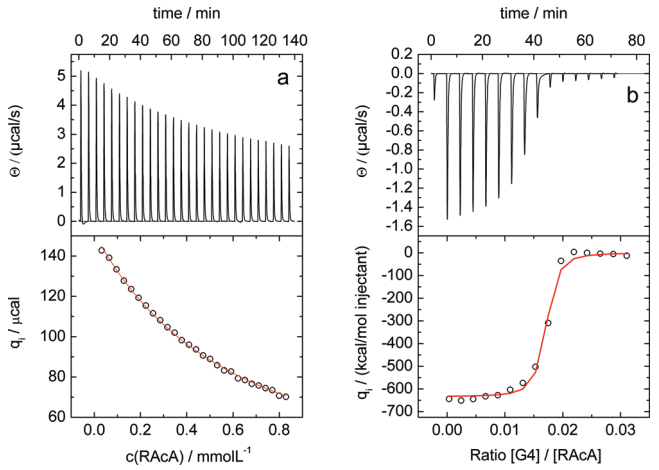

Figure 4. Isothermal titration calorimetry for RAcA: (a) Dilution of RAcA (syringe, c = 6.14 mmol/L) into formic acid buffer (pH = 4); (b) Titration of G4 dendrimer (syringe, c = 5.457 μmolL^{-1}) into RAcA in formic acid buffer (cell, c = 22.15 μmolL^{-1}).

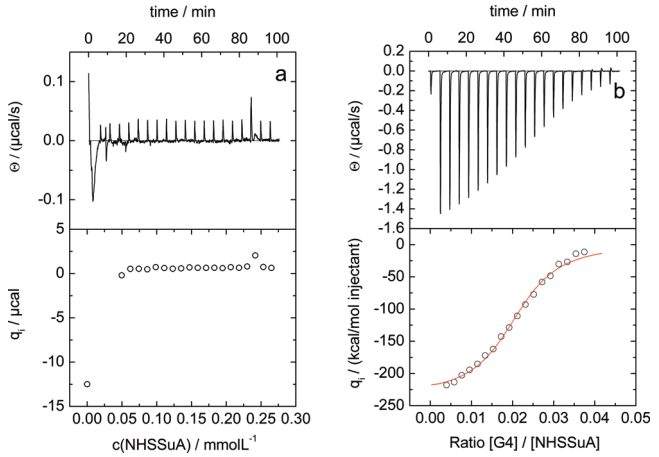

Figure 5. Isothermal titration calorimetry for NHSSuA: (a) Dilution of NHSSuA (syringe, c = 3.578 mmolL^{-1}) in formic acid buffer (pH = 4) into pure buffer; (b) Titration of G4 dendrimer (syringe, c = 37.4 μmolL^{-1}) into NHSSuA (cell, c = 176.1 μmolL^{-1}).

To demonstrate the correlation between structural results and thermodynamic measurements, dilution experiments, and dendrimer titrations are compared for RAcA (Figure 4) and NHSSuA (Figure 5). It is evident from Figure 4a that the dilution of RAcA is a process accompanied by heat uptake, which shows that the dissociation of aggregated dye molecules on dilution is an endothermic process, i.e., formation of dye self-aggregates is exothermal. The stepwise disaggregation model described above fits the data very well and a self-aggregation constant of $K_{\mathrm{dye-dye}} = 2.3 \times 10^2$ L mol^{-1} and an exothermal dye−dye-aggregation energy of $\Delta H_{\mathrm{dye-dye}} = -22.9$ kJmol^{-1} dye result, as is shown in Table 2 where data for all self-aggregating dyes are summarized. From the self-aggregation constant, the free energy can be calculated by means of $\Delta G_{\mathrm{dye-dye}} = -RT \cdot \ln K_{\mathrm{dye-dye}} = -13.4$ kJmol^{-1}, showing that the dye self-aggregation process is entropically disfavored ($T\Delta S_{\mathrm{dye-dye}} = -9.5$ kJmol^{-1}). This is likely due to structural fixation of the dye molecules upon self-aggregation.

Titrating the dendrimer into the dye as depicted in Figure 3b reveals that the dye binding stoichiometry is slightly understoichiometric ($N_{\mathrm{dye}} = 60$). An exothermal association enthalpy of $\Delta H_{\mathrm{dendr-dye}} = -44.3$ kJmol^{-1} and an association equilibrium constant of $K_{\mathrm{dendr-dye}} = 1 \times 10^7$ L mol^{-1} result, which yields a free energy of $\Delta G_{\mathrm{dendr-dye}} = -39.6$ kJmol^{-1}. This shows that the dendrimer-dye association also is entropically disfavored, but not as strongly as the dye self-aggregation. Comparing both experiments is elucidating, as dye self-aggregation and dendrimer-dye-interaction yield valuable insights into the assembly formation process. The comparison shows that for both dye self-aggregation and dendrimer-dye association enthalpy gain is the driving force. For the dye self-aggregation, the enthalpy gain is mostly due to $\pi-\pi$-interactions, while in the dendrimer-dye association, also electrostatic energy by ion-pairing of the positively charged dendrimer amino groups with the negatively charged dye sulfonate groups contributes, leading to a higher dendrimer-dye interaction enthalpy $\Delta H_{\mathrm{dendr-dye}}$. Assuming a comparable value for the $\pi-\pi$-interactions in both processes even though the dye self-aggregation has to overcome the interaction between the like-charged dye molecules, it can be concluded that about 52% of the total interacting enthalpy is contributed by mutual dye−dye-interaction for RAcA. However, the geometry of the dendrimer may also alter the geometry of the dye-aggregates and thus the exact fraction of the interaction enthalpy arising from dye−dye-interaction may deviate from this value.

As NHSSuA was shown not to interconnect the dendrimers into larger assemblies in Section 2.1, comparing the thermodynamic behavior to the results for RAcA is very interesting. ITC titrations of NHSSuA into pure buffer (dilution) and G4 dendrimer into NHSSuA are depicted in Figure 5. It is striking that the dilution curve is completely different from the one of RAcA. After the initial exothermal data point, which can be attributed to adsorption of the dye molecules to the ITC cell wall,[49] the dilution is almost athermal; i.e., no dye self-aggregation occurs. The reason for this can be found in the structure of the molecule, as in general azo dye molecules with separated hydrophilic and hydrophobic or $\pi-\pi$-interacting moieties are more prone to self-interact.[72] The benzene moiety in RAcA is sufficient to enable the dye to develop mutual interactions, whereas NHSSuA does have a charged sulfonate group on the benzene moiety and a charged group on the naphthalene moiety located near the center of the molecule. Therefore, no efficient interaction of the aromatic moieties is possible, as electrostatic repulsion is stronger than for RAcA due to this unfavorable geometry. The dendrimer-dye-interaction further confirms that the binding is much weaker, namely $\Delta H_{\mathrm{dendr-dye}} = -20.2$ kJmol^{-1}, which is only half the value of that of RAcA. Most interestingly, $\Delta H_{\mathrm{dendr-dye}}$(RAcA) and $\Delta H_{\mathrm{dendr-dye}}$(NHSSuA) differ almost exactly by the enthalpic contribution of the dye−dye-interaction of RAcA ($\Delta H_{\mathrm{dendr-dye}}$(RAcA) ≈ $\Delta H_{\mathrm{dendr-dye}}$(NHSSuA) + $\Delta H_{\mathrm{dye-dye}}$(RAcA)), which highlights the decisive role of dye−dye-interaction for the ability of a dye to interconnect the dendrimers. The equilibrium constant and the free energy for NHSSuA are significantly lower than for RAcA ($K_{\mathrm{dye-dye}}$(NHSSuA) = 2 × 10^5 L mol^{-1}; $\Delta G_{\mathrm{dendr-dye}}$(NHSSuA) = −30.6 kJmol^{-1}) and the amount of dye molecules bound per dendrimer $N_{\mathrm{dye}} = 48$ is smaller. The comparison of $\Delta G_{\mathrm{dendr-dye}}$ elucidates that a minimum free energy gain is required to enable a dye to interconnect multiple dendrimers. The smaller amount of dye molecules binding per dendrimer is presumably due to the less expressed dye−dye-interaction not favoring full saturation of the dendrimer.

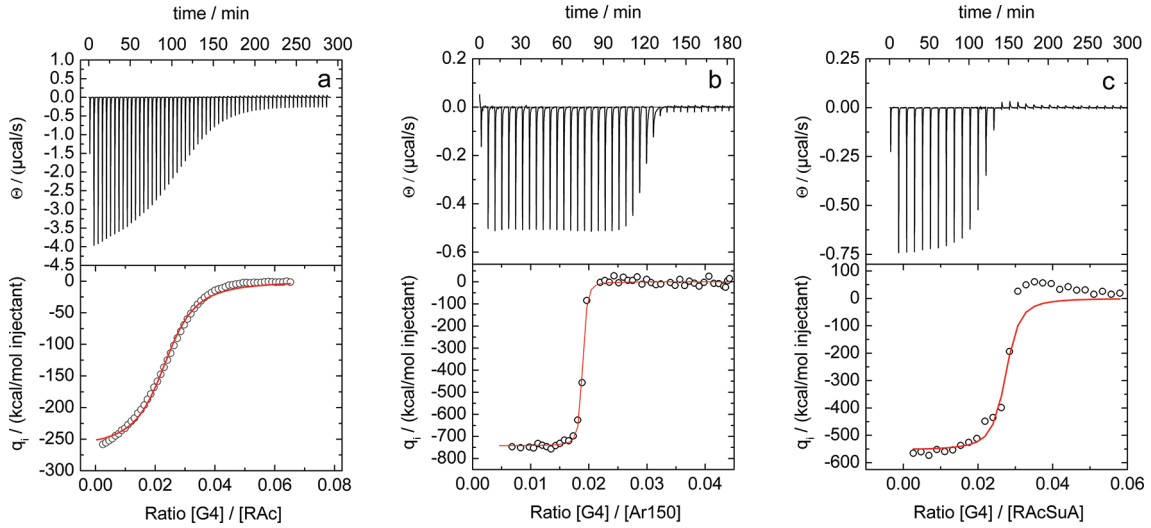

Figure 6. Isothermal titration calorimetry for the titration of G4 dendrimer into (a) RAc, (c_{G4} = 74.86 μmolL^{-1}; c_{RAc} = 253.7 μmolL^{-1}); (b) Ar150, (c_{G4} = 3.40 μmolL^{-1}; c_{Ar150} = 14.47 μmolL^{-1}); (c) RAcA, (c_{G4} = 5.457 μmolL^{-1}; c_{RAcSuA} = 12.61 μmolL^{-1}).

Table 2. ITC Data for the Self-Aggregation of Divalent Azo Dyes

dye	$\Delta H_{dye-dye}$ per dye (kJmol^{-1})	$K_{dye-dye}$ (L mol^{-1})	$\Delta G_{dye-dye}$ (kJ(mol dye)$^{-1}$)	$T\Delta S_{dye-dye}$ (kJ(mol dye) $^{-1}$)
RActBa	−23.7 ± 0.1	(1.5 ± 0.1) × 10^3	−18.0 ± 0.2	−5.7 ± 0.1
Ar150	−22.5 ± 2.1	(1.1 ± 0.3) × 10^4	−23.1 ± 0.9	0.6 ± 0.2
RAcA	−22.9 ± 0.1	(2.3 ± 0.1) × 10^2	−13.4 ± 0.1	−9.5 ± 0.1
Ar26	−30.2 ± 0.2	(3.2 ± 0.2) × 10^3	−19.9 ± 0.1	−10.3 ± 0.1
Ar44	−21.5 ± 1.19	(9.7 ± 0.1) × 10^1	−11.3 ± 0.3	−10.2 ± 0.3

This in turn leaves more dendrimer charges un-neutralized leading to a disfavored dendrimer interconnection. However, the lower binding strength causes more of the initial monovalent counterions and formiate ions of the buffer to remain condensated so that the dendrimer net charge is somewhat smaller than the original charge after subtraction of charges neutralized by dye binding ($q_{dendr,eff} < 126-2N_{dye}$ for divalent dyes). Data show that in the case of NHSSuA the entropic contribution is positive, likely due to the lacking dye−dye-interactions. That is dye stack formation enforces order and causes decreasing entropy, while condensation of nonstacking divalent counterions is entropically favored as in classical polyelectrolyte system such as poly(acrylic acid) interacting with calcium ions.[73]

The ability of RAcA to form assemblies with a hydrodynamic radius of R_H = 24 nm, i.e., an aggregation number of 630 dendrimers per assembly, highlights the importance of the self-interaction of the dye molecules for the formation of nanoscale assemblies. NHSSuA being unable to interconnect the dendrimer shows that a certain minimum of dye−dye self-interaction and dendrimer-dye interaction strength is required for a divalent azo-dye to interconnect dendrimers. This is also in accordance with UV−vis spectroscopy, which showed a strong effect of G4 on the spectrum of RAcA, whereas NHSSuA showed only minor changes. Hence, the assembly formation process can be divided into two hierarchical levels, the first of which is the binding of the dye molecules to the dendrimer and the second one is the interconnection of the individual dendrimer molecules through the dye molecules. Thermodynamic data presented here thus prove that the second hierarchical level is governed by the mutual dye−dye-interaction for divalent dyes. Hence, already based on these results it is evident that there is a clear correlation between dendrimer interconnection ability and thermodynamics.

Figure 6a−c depicts further ITC experiments showing a great variety in binding strength in dependence on the molecular dye structure. The dendrimer-titration of RAc is depicted in Figure 6a. The dye-dilution experiment (not shown) is similar to NHSSuA and the thermodynamic parameters extracted from Figure 6a are in the same range as for NHSSuA as shown in Tables 3a and 3b. This corresponds to the fact that RAc also does not interconnect the dendrimers. In contrast, Ar150 (Figure 6b) shows self-aggregation in the dilution experiment (not shown, data given in Table 2) and the highest values for all dendrimer-dye-interaction parameters, leading to the highest degree of dendrimer interconnection with N_{Den} = 5069. It is surprising that the dye−dye interaction enthalpy of Ar150 is comparable to RAcA even though the aromatic backbone is more extended, but at the same time, the dendrimer-dye interaction is much stronger. This may be due to a more restricted conformation for dye self-aggregates without the dendrimer, causing less contact area between the aromatic domains. Thus a lower self-aggregation energy reduces the enthalpy gain on self-aggregation. However, the self-interaction free energy for Ar150 is the largest among all dyes, as there is no entropy loss ($T\Delta S_{dye-dye}$(Ar150) = 0.6 kJmol^{-1}) in difference to the self-aggregation of all other dyes. That is presumably due to the hydrophobic effect, which results in an entropy gain when the dye molecules aggregate in aqueous solution. This again confirms the connection between dye self-aggregation tendency and dendrimer interconnection ability.

RAcSuA (Figure 6c) is a trivalent dye with the same aromatic structure as RAcA, which does not show dye self-aggregation,

dx.doi.org/10.1021/ja207565m |J. Am. Chem. Soc. 2011, 133, 20341–20356

Table 3a. ITC-Titration Results for Dendrimer-Dye Interaction for Divalent Dyes

dye	$\Delta H_{dendr\text{-}dye}$ (kJ(mol dye)$^{-1}$)	N_{dye} ((mol G4) $^{-1}$)	$K_{dendr\text{-}dye}$ (L mol^{-1})	$\Delta G_{dendr\text{-}dye}$ (kJ(mol dye)$^{-1}$)	$T\Delta S_{dendr\text{-}dye}$ (kJ(mol dye)$^{-1}$)
RActBa	−51.1 ± 0.4	59 ± 3	$(3.0 \pm 0.9) \times 10^7$	−42.9 ± 0.8	−8.2 ± 2.9
Ar150	−53.3 ± 0.8	59 ± 2	$(1.4 \pm 0.6) \times 10^8$	−46.4 ± 1.4	−6.9 ± 3.6
RAcA	−44.3 ± 0.5	60 ± 2	$(1.0 \pm 0.6) \times 10^7$	−39.6 ± 1.6	−4.7 ± 2.5
RAc	−26.4 ± 0.3	42 ± 1	$(8.2 \pm 0.5) \times 10^4$	−28.0 ± 2.6	1.6 ± 1.4
ABDS	−18.2 ± 0.1	52 ± 2	$(5.2 \pm 0.2) \times 10^4$	−26.9 ± 2.1	8.7 ± 1.5
NHSSuA	−20.2 ± 0.3	48 ± 2	$(2.0 \pm 0.5) \times 10^5$	−30.6 ± 0.6	10.4 ± 0.5
Ar26	−49.0 ± 0.8	62 ± 3	$(5.0 \pm 1.5) \times 10^7$	−44.0 ± 0.9	−5.0 ± 3.0
Ar44	−36.6 ± 1.4	62 ± 3	$(3.0 \pm 1.0) \times 10^6$	−37.0 ± 1.6	0.33 ± 0.3
	$\Delta H_{dendr\text{-}sul}$ (kJ(mol sul.)$^{-1}$)	N_{sul}/ mol G4	$K_{dendr\text{-}sul}$ (L mol^{-1})	$\Delta G_{dendr\text{-}sul}$ (kJ(mol sul.)$^{-1}$)	$T\Delta S_{dendr\text{-}sul}$ (kJ (mol sul.)$^{-1}$)
disulfonate[a]	−10.2	43	$2.8 \cdot 10^4$	−25.4	15.2

[a] Averaged ITC-data from ref 49.

Table 3b. ITC-Titration Results for Dendrimer-Dye Interaction for Divalent Dyes Per G4 Dendrimer

dye	$\Delta H_{dendr\text{-}dye}$ (kJ(mol G4)$^{-1}$)	$\Delta G_{dendr\text{-}dye}$ (kJ(mol G4)$^{-1}$)	$T\Delta S_{dendr\text{-}dye}$ (kJ(mol G4)$^{-1}$)
RActBa	−3023 ± 21	−2536 ± 44	−487 ± 113
Ar150	−3133 ± 45	−2727 ± 85	−406 ± 210
RAcA	−2657 ± 27	−2376 ± 96	−281 ± 224
RAc	−1100 ± 11	−1168 ± 190	68 ± 53
ABDS	−940 ± 7	−1387 ± 109	446 ± 77
NHSSuA	−964 ± 13	−1463 ± 28	499 ± 5
Ar26	−3013 ± 47	−2705 ± 60	−308 ± 160
Ar44	−2269 ± 82	−2289 ± 97	20 ± 18

likely due to the stronger repulsion as compared to its divalent counterpart RAcA. Thermodynamic parameters in Tables 4a and 4b show that the binding strength is somewhat higher than that for RAcA, most likely due to the additional charge. Interestingly, the dye is able to form assemblies with a similar hydrodynamic radius as the divalent RAcA. This shows that the three charges prevent the dye from self-aggregation without the presence of the dendrimer, but this repulsion can be overcome if the charges are neutralized by ion-pairing. This is interesting as the additional charge of RAcSuA in comparison to RAcA does not prevent dendrimer interconnection, whereas a charge at the "wrong" position, as for NHSSuA, diminishes the ability of a dye to interconnect dendrimers. Consequently, this finding is in agreement with the observation from UV−vis that strong dye−dye-interaction emerge for Ar150- and NHSSuA-dendrimer assemblies.

It s now of high value to discuss trends of thermodynamics and size in dependence on the dye counterion. ITC data for the dye-dilution experiments and the dendrimer-dye experiments are given in Tables 2−4. It is evident from the amount of dye molecules binding per G4 dendrimer N_{dye} that all divalent dyes capable of self-aggregation bind slightly under-stoichiometrically; i.e., N_{dye} / $N_{stoichiometry}$ = 0.94 to 0.98 dye sulfonate groups bind per dendrimer amino group. Thus a small fraction of dendrimer charges is not neutralized. In contrast, the nonself-aggregating divalent dyes with lower binding strengths to the dendrimer, RAc, ABDS, and NHSSuA, bind significantly under-stoichiometrically, i.e., only 0.67 to 0.83 sulfonate groups bind per amino group. This indicates that lower binding constants $K_{dendr\text{-}dye}$ for nonself-aggregating dyes lead to more unoccupied binding sites on the dendrimer. Due to the much lower extent of dye−dye-interactions of these dyes geometric constraints or lack of mutual interaction may prevent further binding. That is as adjacent dye binding is favored in a cooperative binding process for the first set of dyes, which is most likely not present for this second class of dyes.[72] Further, the initial monovalent counterions have to be displaced from the dendrimer, which is only possible for dye counterions with high binding strengths as the buffer leads to a hundredfold excess of the formiate anions.[74] Thus, the counterion exchange of multivalent dye ions for monovalent ions is not expected to be complete for dyes with low binding strengths. A certain minimum binding strength in the order of $K \approx 10^6$ L mol^{-1} is required for near stoichiometric binding. Consequently, this may in turn be the necessary condition to enable dendrimer interconnection as a strongly self-aggregating dye does not only have a higher tendency to interact mutually, which favors dendrimer interconnection, but also the dye loaded dendrimers have to overcome lower electrostatic repulsion due to a higher degree of charge neutralization. For trivalent dyes, the binding ratio is between 0.9 and 0.93 and thus slightly lower. This may be due to geometric constraints as the additional charge of the trivalent dyes potentially requires more expressed conformation changes of the dendrimer to realize a high number of ion pairs of dye sulfonate and dendrimer amino groups.

The interaction enthalpy for dendrimer-dye-association shows values per dye between $\Delta H_{dendr\text{-}dye}$ = −18 kJmol^{-1} and $\Delta H_{dendr\text{-}dye}$ = −63 kJmol^{-1} for the dendrimer-dye interaction, whereas the entropy is negative for all dyes capable of interconnecting different dendrimers. The dye−dye self-aggregation enthalpy is between $\Delta H_{dye-dye}$ = −21 kJmol^{-1} and $\Delta H_{dye-dye}$ = −30 kJmol^{-1}; i.e., the contribution of the dye−dye-interaction energy to the total dendrimer-dye-energy for divalent dyes is between 42% and 62%. Hence, the main driving force for the dendrimer interconnection is the enthalpy for all dyes. Trivalent dyes show the highest interaction enthalpies per dye due to the additional charge while the aromatic backbone has the same size as for divalent dyes (RAcA compared to RAcSuA). This is in agreement with electrostatic interaction yielding a certain fraction of the total dendrimer-dye interaction energy. However, the dendrimer-dye association process for trivalent dyes is entropically unfavorable and the free energy is comparable to the values for the divalent dyes. As evident from Figure 7, trivalent dyes have a strongly negative entropic contribution, which reduces the

Table 4a. ITC-Titration Results for Dendrimer-Dye Interaction for Trivalent Dyes

dye	$\Delta H_{\text{dendr-dye}}$ (kJmol^{-1})	N_{dye} ((mol G4) $^{-1}$)	$K_{\text{dendr-dye}}$ (L mol $^{-1}$)	$\Delta G_{\text{dendr-dye}}$ (kJ/(mol dye)$^{-1}$)	$T\Delta S_{\text{dendr-dye}}$ (kJ/(mol dye)$^{-1}$)
Ar27	-62.5 ± 0.6	39 ± 1	$(6.0 \pm 3.0) \times 10^7$	-44.4 ± 1.38	-18.1 ± 8.9
Ar18	-58.7 ± 8.8	38 ± 4	$(1.0 \pm 0.6) \times 10^7$	-39.9 ± 10.4	-18.8 ± 5.1
RAcSuA	-62.7 ± 0.7	38 ± 1	$(3.2 \pm 1.4) \times 10^7$	-42.8 ± 3.86	-19.9 ± 9.8

Table 4b. ITC-Titration Results for Dendrimer-Dye Interaction for Trivalent Dyes Per G4 Dendrimer

dye	$\Delta H_{\text{dendr-dye}}$ (kJ(mol G4)$^{-1}$)	$\Delta G_{\text{dendr-dye}}$ (kJ(mol G4)$^{-1}$)	$T\Delta S_{\text{dendr-dye}}$ (kJ(mol G4)$^{-1}$)
Ar27	-2419 ± 21	-1717 ± 51	-702 ± 336
Ar18	-2242 ± 289	-1525 ± 298	-717 ± 191
RAcSuA	-2358 ± 25	-1610 ± 150	-747 ± 376

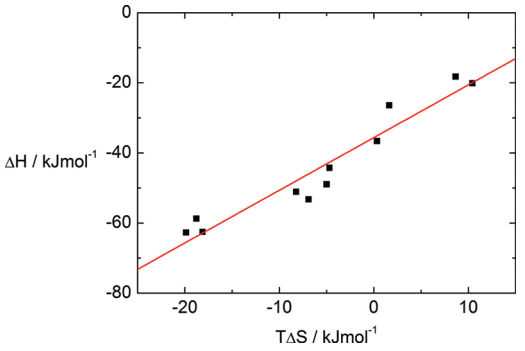

Figure 7. Enthalpy−entropy compensation for dendrimer-dye association.

free energy per dye to values close to the divalent dyes. For example, $\Delta H_{\text{dendr-dye}}$(RAcA) and $\Delta H_{\text{dendr-dye}}$(RAcSuA) differ by 18.4 kJmol^{-1}, but the difference in $\Delta G_{\text{dendr-dye}}$ is only 3.2 kJmol^{-1}. The phenomenon that a large part of an enthalpic gain is not reflected in the free energy but compensated by entropic effects is called enthalpy−entropy compensation and was found in various systems.[75−78] Some authors attributed this to the rearrangement of water molecules in the hydration shell.[78]

Figure 7 displays the enthalpy for the dendrimer-dye interaction on the *y*-axis, the entropy multiplied with the absolute temperature on the *x*-axis and a linear fit of the experimental data.

In literature, often slopes for plots of ΔH versus $T\Delta S$ close to unity are reported, as a large part of enthalpy changes are compensated for by entropy changes with the opposite sign. For example host−guest structures formed by cyclodextrins and guest molecules yield slopes between 1.01 and 1.27.[76] In difference, for the slope of the linear fit in Figure 7, a value close to 1.5 is found, which shows that only a low fraction of the increasing enthalpy gain is compensated for by a counteracting entropy loss. Hence, in the complex system under investigation here, the interplay of interactions does change ΔG, which is the basis for controlling the assembly size through molecular building block choice.

Figure 8 connects the structural results from part 2.1 to the thermodynamic results from this section by plotting the hydrodynamic radii versus enthalpy (8a, 8c) and free energy (8b, 8d) of the dye self-aggregation and the dendrimer-dye association. As mentioned, all divalent dyes for which self-aggregation is found show high binding strengths and the ability to interconnect dendrimers into assemblies. As evident in Figure 8b, an increasing free energy gain leads to larger hydrodynamic radii and thus dendrimer aggregation numbers, whereas non self-aggregating divalent dyes are unable to interconnect dendrimers. Therefore, the latter type of dyes only forms host−guest complexes. The lowest free energy sufficient to induce dendrimer interconnection is $\Delta G_{\text{dendr-dye}} = -37$ kJmol^{-1}, corresponding to $K = 3 \times 10^6$ L mol^{-1} for the dye Ar44. This suggests that a free energy threshold exists below which no interconnection is possible. For the self-aggregating divalent dyes, which can be compared among each other as approximately the same amount of dye counterions bind per dendrimer, linear extrapolation of R_H versus $\Delta G_{\text{dendr-dye}}$ and $\Delta G_{\text{dye−dye}}$ yields fits with high coefficients of determination (r^2) according to eqs 3 and 4. The fit according to eq 3 is also depicted in Figure 8b (red line fitted to black squares):

$$R_H = -93.685 - 3.069\Delta G_{\text{dendr−dye}} \quad (r^2 = 0.946) \qquad (3)$$

$$R_H = -6.062 - 2.398\Delta G_{\text{dye−dye}} \quad (r^2 = 0.976) \qquad (4)$$

This shows that the free energy of both dendrimer-dye interaction and dye-self-aggregation are closely related to the assembly size if only divalent dyes are considered. The free energy extrapolated to the hydrodynamic radius of the dendrimer of R_H = 2.3 nm yields an estimate of the free energy threshold necessary for dendrimer interconnection ($\Delta G_{\text{dendr-dye}} > 31.3$ kJmol^{-1}), which is also indicated in Scheme 2. This threshold is the transition point between the first hierarchical level, i.e. formation of host−guest complexes, and the second level, i.e. interconnection of dendrimers. The onset of dendrimer interconnection depends on the absolute concentration as elucidated in Section 2.1, but even if the concentration is varied, the size differences still correlate with the free energy change.

Thus, if $\Delta G_{\text{dendr-dye}}$ or $\Delta G_{\text{dye−dye}}$ is larger than the threshold, then the hydrodynamic radius increases approximately linearly with ΔG. No dyes were found to yield assemblies with $R_H <$ 20 nm. This may be in analogy to a cooperative binding process where below a certain concentration no complexes form and a sharp transition to high aggregates occurs.[70] Threshold-free energies for the aggregation onset were also found in other self-assembling systems for example in perylene bisimides in organic solvents.[79]

Comparison of Figure 8b,d shows that trivalent dyes cannot be described by the linear approximation, the cause of which likely is connected to the difference in the number of dye counterions bound per dendrimer. This is evident from Figure 8d, where the divalent counterions show the same approximately linear dependency for the free energy per dendrimer as described above per dye, but the trivalent dyes clearly display the influence of the difference in N_{dye}. Figure 8d also shows that for trivalent dyes a smaller energy gain per dendrimer is sufficient to lead to dendrimer interconnection. This difference becomes evident by considering the enthalpy depicted in Figure 8a,c. In Figure 8a, the trivalent dyes show by far the highest enthalpy gain, whereas the value per

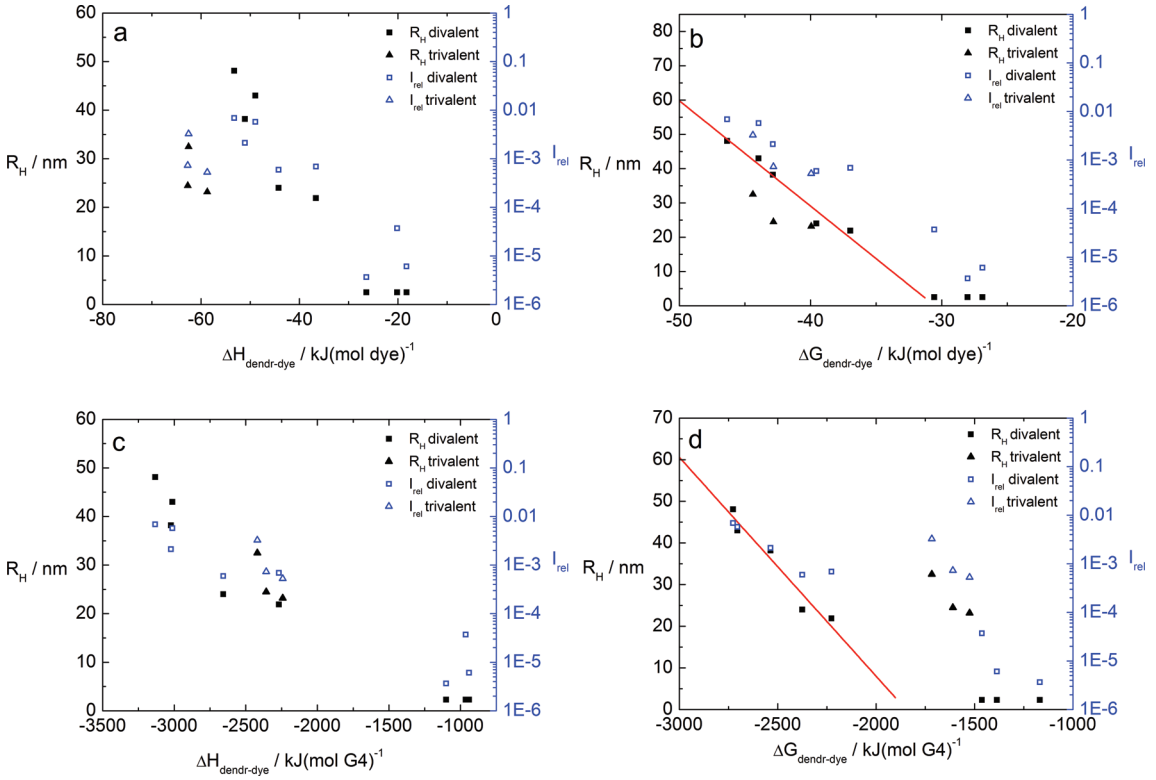

Figure 8. Hydrodynamic radii R_H and relative scattering intensities I_{rel} in dependence on thermodynamic parameters (a) as function of the enthalpy per dye $\Delta H_{dendr\text{-}dye}$, (b) as function of the free energy per dye $\Delta G_{dendr\text{-}dye}$, (c) as function of the enthalpy per dendrimer $\Delta H_{dendr\text{-}dye}$, (d) as function of the free energy per dendrimer $\Delta G_{dendr\text{-}dye}$. Red lines in (b) and (d) represent fits of R_H for the interconnecting divalent dyes (black squares).

Scheme 2. Free Energy Threshold for Host-Guest Complexation As Compared to Dendrimer Interconnection Obtained from Extrapolation of R_H at c_{den} = 0.044 g L^{-1}

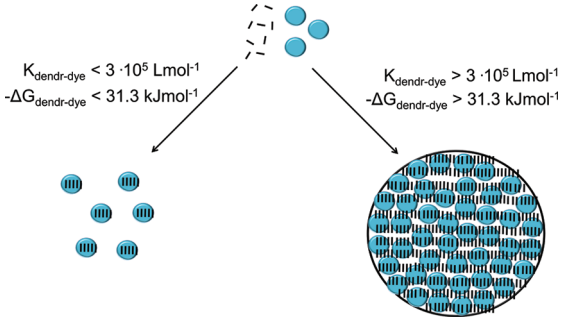

dendrimer is lower than for the divalent dyes due to the lower number of dye molecules binding to each dendrimer.

Figure 9 considers the correlation in more detail by depicting the dendrimer aggregation number N_{Den} in dependence on the enthalpy and free energy changes. The aggregation number increases with the free energy gain in a very similar way for both dendrimer-dye and dye−dye association. Comparison of $\Delta G_{dendr\text{-}dye}$ and $\Delta H_{dendr\text{-}dye}$ highlights again the importance of enthalpy as driving force in, which is in agreement with the finding that the dyes capable of creating assemblies with aggregation numbers $N_{Den} > 1$ have a negative entropic contribution in dendrimer-dye assembly formation.

As general trends, divalent dyes with the charges concentrated in one moiety of the molecule, and thus having unsubstituted aromatic residues like Ar44 and RAcA or aliphatic substituents on the benzene ring (Ar150, Ar26, and RActBa), lead to high free energies of interaction and hence large assemblies of interconnected dendrimers. When the charges are located toward the center of the molecule, smaller assemblies result as found for Ar44 that exhibits a lower dendrimer-dye interaction free energy and smaller aggregation numbers than RAcA, despite the larger aromatic backbone. This shows that more isotropic charge distributions, e.g. the unfavorable position of the charge pointing toward the center of the Ar44 molecule, lead to a lower interaction free energy and thus assembly size. This is further confirmed by NHSSuA having the lowest interaction energy of all naphthalene-benzene based azo dyes of this study and the same finding for the trivalent dye Ar18 in variance to RAcSuA. Overall, it is very interesting that a lower threshold of the free energy enabling dyes to interconnect dendrimers exists, and that a linear dependence of R_H on ΔG and a characteristic dependence of the aggregation number N_{Den} on ΔG was found herein. This will be further discussed in the next section.

2.3. Quantitative Understanding. The final goal of this study is to find a quantitative model linking assembly sizes to thermodynamic parameters. Therefore, it is useful to analyze the contributions to the free energy in more detail to identify an equilibrium condition relating aggregation number and free energy. In a previous study, we determined the binding parameters of different nonaromatic alkyldisulfonates to the dendrimer, so that the electrostatic part of the dendrimer-dye association free energy can be estimated from those data.[49] Disulfonates are flexible as opposed to the dye molecules where the sulfonates are rigidly fixed by the aromatic backbone. Nevertheless, the number of

dx.doi.org/10.1021/ja207565m |J. Am. Chem. Soc. 2011, 133, 20341–20356

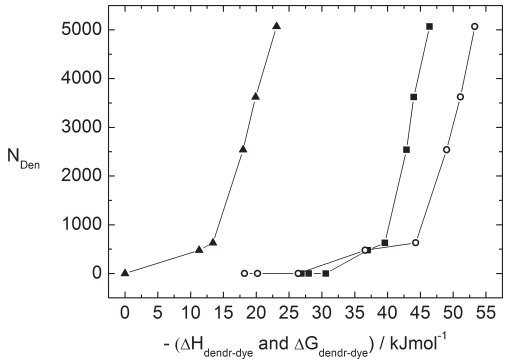

Figure 9. Dendrimer aggregation number N_{Den} in dependence on dendrimer-dye interaction free energy $\Delta G_{dendr\text{-}dye}$ (squares) and enthalpy $\Delta H_{dendr\text{-}dye}$ (open circles) and dye−dye interaction free energy $\Delta G_{dye-dye}$ (triangles) for divalent dyes.

charges is the same and thus a valuable estimate can be made for the contribution of the electrostatic interaction to the binding process. For this estimation, the averaged binding parameters of the disulfonates determined in ref 49 are included in Table 3a.

Pure electrostatic binding leads to moderate binding strengths in the order of magnitude of $K_{dendr\text{-}sul} = 2.8 \times 10^4$ L mol^{-1} and an enthalpy and free energy of about $\Delta H_{dendr\text{-}sul} = -10$ kJmol^{-1} and $\Delta G_{dendr\text{-}sul} = -25$ kJmol^{-1}. That is, the binding to the dendrimer is entropically favored. As described by Antonietti et al. binding of calcium ions to poly(acrylic acid) is entropically favored due to the release of the initial monovalent counterions which is also accompanied by changes in the water structure.[73] This is in agreement with the entropy change in the present electrostatic system. Neither of the previously investigated disulfonates interconnected the dendrimers to a considerable extent, which is in accordance with the low binding strength in the order of nonself-aggregating dyes far below the free energy threshold. Another interesting point is the free energy and equilibrium constant of nonaromatic disulfonate-dendrimer association being in the same range as for the noninterconnecting dyes NHSSuA, ABDS and RAc. This is a further proof that non self-aggregating divalent dyes are unable to develop strong mutual interactions when binding to the dendrimer, indicating noncooperative binding. In addition, this is also evident from the weak interaction estimated from UV−vis spectroscopy. As all those dyes bind under-stoichiometrically to the dendrimer, a certain strength of binding is required to almost fully saturate the dendrimer when the monovalent counterions or the buffer ions originally present in the dendrimer have to be exchanged. Only a nearly fully saturated dendrimer is able to become interconnected.

As pointed out, the attractive component of the total interaction free energy is mainly composed of the electrostatic interaction (ΔG_{elec}) and the secondary dye−dye interaction (ΔG_{sec}) and thus:

$$\Delta G_{dendr-dye} = \Delta G_{elec} + \Delta G_{sec} \quad (5)$$

The electrostatic interaction ΔG_{elec} comprises interactions between charges, entropic contributions from the release of initial counterions and changes in solvation of the ionic sulfonate groups. ΔG_{sec} consists of $\pi-\pi$-interactions, hydrophobic interactions and eventually further contributions like cation-π interactions. The equilibrium constant can be written as follows:

$$K_{dendr-dye} = K_{elec} \cdot K_{sec} \quad (6)$$

To establish a model based on the data presented, ΔG_{elec} is approximated with $\Delta G_{dendr\text{-}sul}$ and ΔG_{sec} with the dye self-aggregation free energy $\Delta G_{dye-dye}$. Only divalent dyes can be considered, as only for these the nonaromatic disulfonate is an appropriate approximation for the electrostatic contribution:

$$\Delta G_{dendr\text{-}dye} = \Delta G_{dendr\text{-}sul} + \Delta G_{dye\text{-}dye} \quad (7)$$

Equation 7 neglects several contributions, e.g., cation-π-interactions and geometric effects of the counterions on the formation of dendrimer-dye nanostructures. However, other contributions mentioned above such as possible hydrophobic effects or changes in the water structure that occur upon dye stacking are directly included in the substitution of ΔG_{sec} through $\Delta G_{dye-dye}$. To validate this approach, the free energy change $\Delta G_{dendr\text{-}dye}$ measured directly from dendrimer-dye ITC experiments (Table 3) can be compared to the free energy calculated according to eq 7. It turns out that the free energy calculated by adding the free energy of disulfonate binding to the free energy of dye−dye-interaction is in very good agreement with the dendrimer-dye interaction energy as determined from the direct ITC measurement (Table 5).

Therefore the equilibrium constant may be expressed as follows:

$$K_{dendr\text{-}dye} = K_{dendr\text{-}sul} \cdot K_{dye\text{-}dye} \approx K_0 \cdot q \quad (8)$$

K_0 thereby is the nucleation constant and q the cooperativity parameter in the cooperative binding of dyes to polyelectrolytes as described by Schwarz.[70,80] As the binding of the disulfonate to the dendrimer is noncooperative due to the disulfonates lacking self-interaction, the dye−dye-interaction comprises all mutual interactions between the dye counterions. Thus $K_{dendr\text{-}sul}$ can be compared to the nucleation constant of a cooperative binding process according to Schwarz, whereby $K_{dye-dye}$ is in analogy to the cooperativity parameter.[70,71] Therefore, the cooperativity of the dye-binding is directly connected to the ability of the dyes to interconnect the dendrimer molecules. For $\Delta G_{dye-dye} = 0$, the cooperativity parameter is unity and no interconnection of dendrimers can occur for divalent ions. If the dendrimer-dye assemblies are considered as equilibrium structures, then the condition for the finite aggregate size of the dye-loaded dendrimer-assemblies is as follows:

$$\Delta G_{attraction} + \Delta G_{repulsion} = 0 \quad (9)$$

Hence, the assembly growth ceases once the free energy of attraction equals the free energy of repulsion. The repulsive term of the free energy $\Delta G_{repulsion}$ can be approximated to arise from Coulomb repulsion of dye-loaded dendrimers becoming interconnected. This is reasonable as assembly formation depends strongly on the ratio of charges and full neutralization of the charged components leads to precipitation rather than the formation of finite-sized assemblies. Scheme 3 depicts the situation when an aggregate is formed: The dye counterions bind cooperatively to the dendrimer, reducing its initial charge $q_{dendrimer,0}$. On interconnection, the dendrimers carry a residual charge $q_{dendrimer}$ and therefore the interconnection of individual dendrimers leads to accumulation of charge in the assembly. The residual charge per dendrimer can be calculated as $q_{dendrimer} = 126 - 2\,N_{dye} \approx 11$ for the loading ratio of $l = 1.8$ and $N_{dye} = 57$ in this study. The value of $N_{dye} \approx 57$ deduced from the loading ratio will be used as an approximation for all dyes. Possible contributions of condensed monovalent counterions and a heterogeneous dye distribution are neglected. In a simplified fashion, the repulsive contribution can

Table 5. Thermodynamic Data for Dye Self-Aggregation and Disulfonate Binding to the Dendrimer in Comparison with the Dendrimer-Dye Association

dye	$K_{dye-dye} \times K_{dendr-sul}$ (L^2mol^{-2})	$K_{dendr-dye}$ ($L\ mol^{-1}$)	($\Delta G_{dye-dye}$+ $\Delta G_{dendr-sul}$) (kJ(mol dye)$^{-1}$)	$\Delta G_{dendr-dye}$ kJ ((mol dye) $^{-1}$)	$\Delta H_{dye-dye}/\Delta H_{dendr-dye}$
RActBa	4.0×10^7	$(3.0 \pm 0.9) \times 10^7$	−43.4	−42.9 ± 0.8	0.46
Ar150	3.1×10^8	$(1.4 \pm 0.6) \times 10^8$	−48.5	−46.4 ± 1.4	0.42
RAcA	6.3×10^6	$(1.0 \pm 0.6) \times 10^7$	−38.8	−39.6 ± 1.6	0.52
Ar26	8.6×10^7	$(5.0 \pm 1.5) \times 10^7$	−45.3	−44.0 ± 0.9	0.62
Ar44	2.7×10^6	$(3.0 \pm 1.0) \times 10^6$	−36.7	−37.0 ± 1.6	0.59

be expressed by considering a growing aggregate starting with one dye-loaded dendrimer that approaches another dye-loaded dendrimer from infinite distance, which requires the electrostatic energy for two point charges that approach each other. Then, further dendrimers attach to the assembly in steps (i) until $N_{Den} - 1$ dendrimers are added to the initial dendrimer for the particular assembly. This consideration leads to the following:

$$\Delta G_{repulsion} = \frac{1}{4\pi\varepsilon_0\varepsilon_r} \cdot \sum_{i=1}^{N_{Den}-1} \frac{Q_{assembly}(i) q_{dendrimer}}{r(i)} \qquad (10)$$

$Q_{assembly}$ is the charge of the growing assembly at an aggregation number $i < N_{Den}$, $r(i)$ the distance of the centers of the assembly and the dendrimer upon attachment. In addition, the dielectric constant of the aqueous solution is approximated with the value for pure water, $\varepsilon_r = 80$. The net charge of the growing assembly can be calculated as the sum of the estimated residual dendrimer charges:

$$Q_{assembly}(i) = q_{dendrimer} \cdot i \qquad (11)$$

The distance between the center of the molecules is calculated as follows:

$$r(i) = R_{H\text{-}ass}(i) + R_{H\text{-}den} = R_{H\text{-}den} \cdot (\sqrt[3]{i} + 1) \qquad (12)$$

As the assembly consists of ionic species and is swollen with the solution containing further ions, instead of pure Coulomb interaction as in eq 10, screened Coulomb interaction according to the Debye−Hückel approach is included

$$\Delta G_{repulsion} = \frac{q^2_{dendrimer}}{4\pi\varepsilon_0\varepsilon_r R_{H-den}} \cdot \sum_{i=1}^{N_{Den}-1} \left(\frac{i}{\sqrt[3]{i} + 1} \exp(-\kappa(\sqrt[3]{i} + 1) R_{H-den}) \right) \qquad (13)$$

where κ is the inverse Debye screening length. Describing the interaction of charged spheres as overlap of two screened coulomb potentials, also known as Yukawa potential and for example commonly used in the DLVO approach for the description of colloidal systems, of course represents a rough estimate as it is well-known that this is not appropriate for many charged particle systems, even in cases of spherical model macroions.[81−83] Hence, it cannot be expected to quantitatively hold in this much more complex system, but seems well-suited for a general simplified consideration.

Further, an expression for the free energy of attraction $\Delta G_{attraction}$ can be derived from the free energy for the dendrimer-dye interaction $\Delta G_{dendr-dye}$. For the divalent dyes, variations in $\Delta G_{dendr-dye}$ arise mainly from the difference in dye−dye-interactions

Scheme 3. Assembly Formation Model

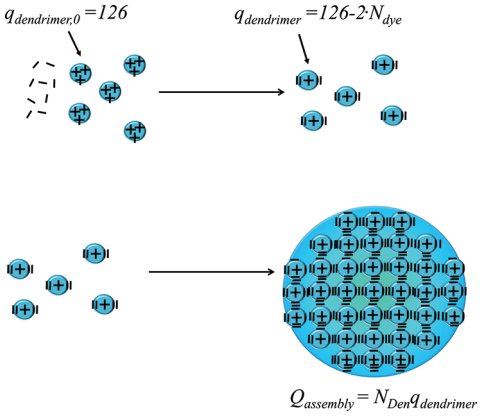

$\Delta G_{dye-dye}$, whereas the electrostatic contribution approximated by $\Delta G_{dendr-sul}$ is almost constant for all dyes. The attractive free energy is thus obtained by adding the free energy gain for all dendrimer-dye interactions formed in the assembly:

$$\Delta G_{attraction} = N_{Den} N_{dye} \Delta G_{dendr-dye} \qquad (14)$$

$$\Delta G_{attraction} = N_{Den} N_{dye} \cdot (\Delta G_{dendr-sul} + \Delta G_{dye-dye}) \qquad (15)$$

In combination, attractive and repulsive free energy yield the equilibrium condition,

$$\frac{(126 - 2N_{dye})^2}{4\pi\varepsilon_0\varepsilon_r R_{H-den}} \cdot \sum_{i=1}^{N_{Den}-1} \left(\frac{i}{\sqrt[3]{i} + 1} \exp(-\kappa(\sqrt[3]{i} + 1) R_{H-den}) \right) + N_{Den} \cdot N_{dye} (\Delta G_{dendr-sul} + \Delta G_{dye-dye}) = 0 \qquad (16)$$

Hence, an equilibrium condition results that relates the number of dendrimers per assembly, i.e., the aggregation number N_{Den} with the number of dye molecules per dendrimer N_{dye} and the dendrimer dye interaction energy, here expressed as the sum of the ionic and the interdye interaction free energy $\Delta G_{dendr-sul}$ + $\Delta G_{dye-dye}$. Thus, given a set of the latter three parameters characteristic for a certain macroion-dye system, a particular finite aggregation number results. Thereby, the experimental observation of the formation of assemblies with finite and defined size can be explained by this facile model of equilibrating attraction and repulsion. Furthermore, for the model system of divalent dyes considered here, a constant $\Delta G_{dendr-sul}$, and N_{dye} can be assumed and hence eq 16 relates the aggregation number directly and solely to the dye−dye free interaction energy. This, again, is consistent with the experimental observation that $\Delta G_{dye-dye}$, is the crucial factor in determining the assembly size. Applying

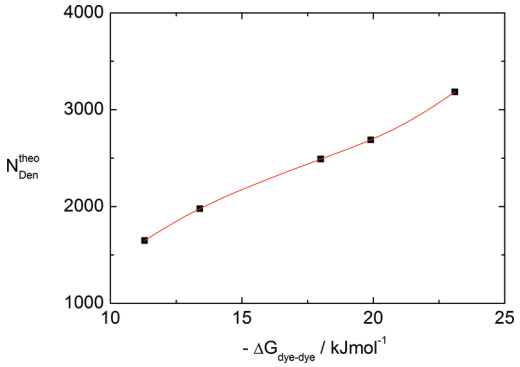

Figure 10. Calculated aggregation number for the different dyes as function of the dye−dye interaction free energy.

eq 16 to the experimental values of the dendrimer-dye interaction free energies for the various dyes with the screening length κ as fitting parameter results in calculated aggregation numbers as given in Figure 10.

Evidently, the model is able to represent the aggregation number increase with increasing $\Delta G_{dye-dye}$. However, the experimental relationship (Figure 9) quantitatively shows a stronger dependence on interaction energy than the model in its current status. Equalizing experimental and calculated aggregation numbers results in the need for a further dye-dependent correction factor ranging from 0.3 for Ar44 to 1.7 for Ar150. This is due to factors not considered in the facile model which may have their origin for example in a nonhomogeneous distribution of dye molecules among dendrimers or a varying shape of the assemblies. A higher $\pi-\pi$ interaction strength is expected to result in more anisotropic assemblies, i.e., a different translation of R_h into aggregation number. Yet the fact that an aggregation number dependency extracted from scattering intensities is very similar to the one extracted from hydrodynamic radii indicates that this effect is not too influencing.

The fact that the dye−dye-interaction free energy plays the dominant role for the dendrimer interconnection can be understood as follows: When a dye-loaded dendrimer becomes attached to a large assembly, the free energy released is mainly due to dye−dye-interactions because the attractive ionic dye−dendrimer interaction is already in place. But dye-loaded dendrimers contain rather short columnar dye stacks so that merging of stack ends is favored through the free energy gain of dye−dye-interaction. Thus, the total dye−dye-interaction in individual dendrimers is smaller due to such end effects, i.e. stack lengths are confined to the diameter of a single dendrimer. This restriction is relieved when larger assemblies form. This attractive effect has to compensate for the electrostatic repulsion arising from the repulsion of like-charged dye-loaded dendrimer species. Hence, equilibration of these interplaying effects occurs at a certain assembly size, i.e., aggregation number. In a broader sense this may be seen as in accordance with calculations by Douglas et al. who also considered the balance between interplaying interactions as important for the formation of ordered structures through supramolecular self-assembly.[84,85] In analogy, but in a very different system, it was shown by theoretical considerations that for a suspension of charged colloidal particles the interplay of repulsive screened electrostatic and short-range attractive interactions can lead to defined structure.[86] More specifically, a stabilization of charged assemblies through a net charge of the assembly that is caused through secondary effects—e.g., finite size counterions as opposed to point-like counterions—was theoretically discussed for biomacromolecule bundles by Pincus et al., and in terms of somewhat different equilibria by Holm et al.[32,87] However, despite ongoing and recent effort from the theory side, a quantitative and comprehensive understanding of self-assembled systems, in particular of such involving multiple interaction types and especially of those based on ionic effects does not yet exist. But for a targeted structure design and for exploiting the large potential of self-assembled structures in applications ranging from medicine to nanoelectronics, understanding structure formation will be essential. Hence, the systematic model system data set on electrostatically self-assembled nanoparticles presented herein may represent a key step toward developing such fundamental insight and thereby a molecular toolbox which allows to build specific nanoscale particles with a desired size, architecture, and function.

3. CONCLUSIONS

We have demonstrated that thermodynamic measurements lead to a very good understanding of driving forces and size control in electrostatic self-assembly of dendrimer macroions and multivalent ionic dye molecules into well-defined supramolecular nanoparticles of adjustable size. Structural features of azo dyes such as charge positioning or substitution with alkyl groups were related to the final assembly size. Dyes with hydrophobic moieties spatially separated from the charged groups yield assemblies of larger size than more isotropic dye counterions. Unfavorable charge positioning in dye molecules leads to the formation of host−guest complexes rather than assemblies of interconnected dendrimers. On the basis of thermodynamic measurements, a correlation between the free energy of association and the assembly size (aggregation number) was revealed. The existence of a free energy threshold for dendrimer interconnection was elucidated, below which no interconnection of the dendrimers took place. A simple attraction−repulsion model was introduced providing quantitative understanding of the finite assembly size. Further, on the basis of the free energy of dye−dye association, the resulting dendrimer−dye assembly size can now be predicted, which is a key step to a molecular toolbox that allows for a targeted structure design.

4. EXPERIMENTAL SECTION

4.1. Chemicals. Polyamidoamine dendrimer of generation 4 was obtained from Dendritech, Midland, MI, USA. Radius and size distribution given by the supplier were confirmed by DLS and HPLC. Acid Red dyes were obtained from Acros, Geel, Belgium (Ar26, Ar44, Ar27, Ar18, Ar150) and building blocks for synthesis in >95% purity from Aldrich, Schnelldorf, Germany (Disodium 3-hydroxy-naphthalene-2,7-disulfonate (R-Acid sodium salt, (RAc)); sodium-7-hydroxynaphthalene-1-sulfonate, (NHS); Aniline (A); 4-*tert*-butylaniline (*t*Ba); sulfanilic acid (SuA). Purification of the dyes was achieved as described below.

4.2. Dye Synthesis. I. The dyes RAcA (disodium 4-(phenyldiazenyl)-3-hydroxynaphthalene-2,7-disulfonate), RActBa (Disodium 4-((4-(*tert*-butyl)phenyl)diazenyl)-3-hydroxynaphthalene-2,7-disulfonate), RAcSua (disodium 4-((4-sulfonatophenyl)diazenyl)naphthalene-2−7-disulfonate) and NHSSuA (disodium 8-(4-sulfonatophenyl)diazenyl-7-hydroxynaphthalene-1-sulfonate) were synthesized by azo-coupling of RAc and NHS with aniline, 4-*tert*-butylphenylaniline and sulfanilic acid:[88]

4.2.1. Diazotation. Fifteen mmol of the diazotation component (aniline, 4-tertbutylphenylaniline or sulfanilic acid) were dissolved in 100 mL 6N HCl under cooling on an ice-bath. Fifteen mmol of sodium

nitrite were dissolved in 100 mL Milli-Q water and added dropwise to the first solution under stirring at 0 °C. The reaction mixture was stirred until the test for nitrite with iodine-starch paper was negative. If after two hours residual nitrite was present, then it was captured by addition of sulfamic acid.

4.2.2. Azo-Coupling. Fifteen mmol of the sodium salt of R-Acid or NHSSuA were dissolved in 180 mL 2N sodium carbonate solution containing enough sodium hydroxide to neutralize the hydrochloric acid in the reaction mixture from step (a) and to adjust the reaction mixture to a pH of 8. The reaction mixture from step (a) was poured into the solution from step (b) under vigorous stirring and ice-cooling after which it immediately turned red or orange. After CO_2-evolution had finished, the reaction mixture was stirred for several hours after removing the ice-bath. The product precipitated immediately or after reducing the volume by rotational evaporation and was collected readily on a Buchner funnel.

4.2.3. Purification:[89] The crude product was purified by dissolving it in just enough water required for full dissolution and subsequent boiling for 5−10 min. After that, 40 wt% sodium acetate solution was added to precipitate the compound and the solution was allowed to stand in an ice-bath for 20 min. The resulting precipitate was collected on a Buchner funnel and the procedure repeated 5−6 times. To remove the sodium acetate, the product was recrystallized from absolute ethanol for 5−6 times and dried in vacuum at 50 °C for 5 days at 10^{-3} mbar. On addition of silver nitrate no precipitate can be observed, showing that the product is free of the potential inorganic contaminants NaCl and Na_2CO_3. The product is also free of detectable organic impurities as shown by UV−vis, ^{1}H NMR and elemental analysis.

4.2.4. Characterization. Yields were calculated on basis of carbon content from elemental analysis. NMR-spectra showed that the product is salt-free except for <2 w% sodium acetate and a small amount of ethanol <2 wt% which could not be removed despite prolonged drying at high vacuum. The purities given below are corrected for residual amounts of sodium acetate and ethanol, which were determined by NMR. Azo-dyes are known to possess multiple molecules of crystal water.[90] Thus, the pure dye contents are below 96%, which does not indicate impurities.

1. RAcA: Elemental analysis: Found: C: 39.81%, Calculated: C: 42.48%, dye-content: 91%. ^{1}H NMR (D_2O, 300 MHz): δ = 7.72 (d, 1H), 7.60 (dd, 1H), 7.35 (s, 1H), 7.12 (s, 1H), 6.95 (t, 3H), 6.70 (d, 2H). UV−vis: $\varepsilon(\lambda = 491\ \text{nm}) = 20\,856\ \text{L(mol·cm)}^{-1}$. ESI-MS: m/z = 428.8 (RAcA − Na).

2. RActBa: C: 43.89%, Calculated: C: 47.24%, dye-content: 91%. ^{1}H NMR (D_2O, 300 MHz): δ = 7.93 (d, 1H), 7.65 (d, 1H), 7.16 (s, 1H), 7.03 (s, 1H), 6.92 (d, 2H), 6.40 (d, 2H), 1.15 (s, 9 H). UV−vis: $\varepsilon(\lambda = 499\ \text{nm}) = 23\,532\ \text{L L(mol·cm)}^{-1}$. ESI-MS: m/z = 484.9 (RActBa − Na).

3. RAcSua: C: 30.65%, Calculated: C: 34.66%, dye-content: 85%. ^{1}H NMR (D_2O, 300 MHz): δ = 8.00 (d, 1H), 7.82 (s, 1H), 7.73 (dd, 1H), 7.55 (m, 3H), 7.24 (d, 2H). UV−vis: $\varepsilon(\lambda = 489\ \text{nm}) = 22529\ \text{L(mol·cm)}^{-1}$. ESI-MS: m/z = 530.9 (RAcSua − Na).

4. NHSSuA: C: 39.90%, Calculated: C: 42.48%, dye-content: 94%. ^{1}H NMR (D_2O, 300 MHz): δ = 8.15 (dd, 1H), 7.85 (d, 2H), 7.70 (d, 2H), 7.28 (s, 1H), 6.41 (d, 1H). UV−vis: $\varepsilon(\lambda = 478\ \text{nm}) = 23199\ \text{L(mol·cm)}^{-1}$. ESI-MS: m/z = 428.8 (NHSSuA − Na).

II. ABDS (4,4′-azobenzenedisulfonate) was synthesized by oxidation of sulfanilic acid by sodium hypochlorite according to a procedure by Clark and obtained in 85% dye content.[91]

4.3. Sample Preparation. Stock solutions were prepared in Milli-Q water (>18.2 MΩ/cm) at the desired pH where the PAMAM dendrimer is fully deprotonated (pH = 10.5). pH-values were adjusted by adding NaOH or HCl standard solutions. All pH-values were counter-checked by a freshly calibrated pH-electrode. An aqueous solution of the dye at pH = 10.5 was diluted with Milli-Q water adjusted to pH = 10.5. Dendrimer stock solution at the same pH was added. After mixing, the appropriate amount of HCl was added at once under turbulent mixing to adjust the sample pH to 3.5 inducing assembly formation.

4.4. Light Scattering. Measurements were carried out using an ALV 5000 correlator with 320 channels, a CDS 3 goniometer (ALV Langen, Germany) and a HeNe laser with a wavelength of λ = 632.8 nm with 22 mW output power. A range of scattering angles of $30° \le \theta \le 150°$ was covered. The intensity autocorrelation function was transferred into the electric field autocorrelation function, which was then analyzed via regularized inverse Laplace transformation using the program CONTIN. This results in a distribution of relaxation times. The widths of the size distribution is given by the standard deviation σ of the intensity weighted relaxation time distribution with logarithmic τ-axis. The apparent diffusion coefficient is then calculated from the mean relaxation time using the relation $D_{app} = q^{-2}\tau^{-1}$. D_{app} was extrapolated to zero scattering vector square and D^0_{app} converted to the hydrodynamic radius using the Stokes−Einstein relationship. The standard concentration of PAMAM dendrimer was c = 0.045 g L^{-1}.

4.5. ζ-Potential. ζ-Potential measurements were conducted on a DelsaNano C Particle Analyzer (Beckmann Coultier). Usually 3 runs were used and the electrophoretic mobility was transferred into into the ζ-potential as introduced by Oshima.[92,93]

4.6. UV−vis Spectroscopy. Absorption spectra were recorded on a Varian Cary 5000 spectrometer using quartz cuvettes with 1 cm path length at dye concentrations of $c \approx 2.5 \times 10^{-5}$ molL^{-1}.

4.7. Isothermal Titration Calorimetry. ITC-measurements were carried out with a VP-ITC microcalorimeter from Microcal Inc. (Northampton, MA). For the dye-dilution experiments, one initial injection of 10 μL to saturate the titration cell wall was followed by 20 injections of 5 μL each. Dilution heats of PAMAM dendrimer were negligible in comparison to dendrimer-dye-interaction energies. The timespan between subsequent injections was 300 s. All experiments were conducted at 25 °C. For dendrimer-dye experiments 15 to 50 injections of 5−15 μL each were used. The timespan between subsequent injections was 300 s. All experiments were conducted at 25 °C. Formic acid/formiate was used as buffer system with c(buffer) = 15 mmol. The buffer was adjusted to pH = 4 by addition of the calculated amount of 1N sodium hydroxide and the final pH checked by a pH-electrode. Data analysis for dendrimer-dye experiments was performed using a one-site model as implemented in MicroCal ITC data analysis software for Origin 7.0.

AUTHOR INFORMATION

Corresponding Author
franziska.groehn@chemie.uni-erlangen.de

ACKNOWLEDGMENT

Financial support of the German Science Foundation (DFG), Verband der Chemischen Industrie (VCI) and the Interdisciplinary Center for Molecular Materials (ICMM, University Erlangen-Nürnberg) is gratefully acknowledged. We are thankful to Thomas Drewello and Claudia Dammann for recording ESI-MS and to Markus Berger for NMR-spectra. Torben Schindler is gratefully acknowledged for experimental help.

REFERENCES

(1) Ringsdorf, H.; Schlarb, B.; Venzmer, J. *Angew. Chem., Int. Ed.* **1988**, *27*, 113–158.
(2) Lehn, J. M. *Angew. Chem., Int. Ed.* **1988**, *27*, 89–112.
(3) Pochan, D. J.; Chen, Z. Y.; Cui, H. G.; Hales, K.; Qi, K.; Wooley, K. L. *Science* **2004**, *306*, 94–97.
(4) Kaiser, T. E.; Wang, H.; Stepanenko, V.; Würthner, F. *Angew. Chem., Int. Ed.* **2007**, *46*, 5541–5544.

(5) Elmahdy, M. M.; Dou, X.; Mondeshki, M.; Floudas, G.; Butt, H. J.; Spiess, H. W.; Müllen, K. *J. Am. Chem. Soc.* **2008**, *130*, 5311–5319.
(6) Smulders, M. M. J.; Schenning, A. P. H. J.; Meijer, E. W. *J. Am. Chem. Soc.* **2008**, *130*, 606–611.
(7) Lee, E.; Kim, J. K.; Lee, M. *Angew. Chem., Int. Ed.* **2008**, *47*, 6375–6378.
(8) Willerich, I.; Gröhn, F. *Angew. Chem., Int. Ed.* **2010**, *49*, 8104–8108.
(9) Gröhn, F. *Soft Matter* **2010**, *6*, 4296–4302.
(10) Sijbesma, R. P.; Beijer, F. H.; Brunsveld, L.; Folmer, B. J. B.; Ky Hirschberg, J. H. K.; Lange, R. F. M.; Lowe, J. K. L.; Meijer, E. W. *Science* **1997**, *278*, 1601–1604.
(11) Beck, J. B.; Rowan, S. J. J. *Am. Chem. Soc.* **2003**, *125*, 13922–13923.
(12) Northrop, B. H.; Zheng, Y.-R.; Chi, K.-W.; Stang, P. J. *Acc. Chem. Res.* **2009**, *42*, 1554–1563.
(13) Gröger, G.; Meyer-Zaika, W.; Böttcher, C.; Gröhn, F.; Ruthard, C.; Schmuck, C. *J. Am. Chem. Soc.* **2011**, *133*, 8961–8971.
(14) Yang, Z.; Galloway, J. A.; Yu, H. *Langmuir* **1999**, *15*, 8405–8411.
(15) Faul, C. F. J.; Antonietti, M. *Chem.—Eur. J.* **2002**, *8*, 2764–2768.
(16) Zhang, Y.; Guan, Y.; Yang, S.; Xu, J.; Han, C. C. *Adv. Mater.* **2003**, *15*, 832–834.
(17) Xu, Y.; Bolisetty, S.; Ballauff, M.; Müller, A. H. E. *J. Am. Chem. Soc.* **2009**, *131*, 1640–1641.
(18) Loizou, E.; Porcar, L.; Schexnailder, P.; Schmidt, G.; Butler, P. *Macromolecules* **2010**, *43*, 1041–1049.
(19) Yan, M.; Fresnais, J.; Berret, J.-F. *Soft Matter* **2010**, *6*, 1997–2005.
(20) Zhou, S.; Burger, C.; Chu, B.; Sawamura, M.; Nagahama, N.; Toganoh, M.; Hackler, U. E.; Isobe, H.; Nakamura, E. *Science* **2001**, *291*, 1944–1947.
(21) Discher, D. E.; Eisenberg, A. *Science* **2002**, *297*, 967–973.
(22) Antonietti, M.; Förster, S. *Adv. Mater.* **2003**, *15*, 1323–1333.
(23) Nikolic, M. S.; Olsson, C.; Salcher, A.; Kornowski, A.; Rank, A.; Schubert, R.; Frömsdorf, A.; Weller, H.; Förster, S. *Angew. Chem., Int. Ed.* **2009**, *48*, 2752–2754.
(24) DeMuth, P. C.; Su, X.; Samuel, R. E.; Hammond, P. T.; Irvine, D. J. *Adv. Mater.* **2010**, *22*, 4851–4856.
(25) White, R. J.; Tauer, K.; Antonietti, M.; Titirici, M.-M. *J. Am. Chem. Soc.* **2010**, *132*, 17360–17363.
(26) Gröhn, F; Klein, K.; Koynov, K. *Macromol. Rapid Commun.* **2010**, *31*, 75–80.
(27) Domes, S.; Filiz, V.; Nitsche, J.; Frömsdorf, A.; Förster, S. *Langmuir* **2010**, *26*, 6927–6931.
(28) Glotzer, S. C. *Science* **2004**, *306*, 419–420.
(29) Glotzer, S. C.; Solomon, M. J. *Nat. Mater.* **2007**, *6*, 557–562.
(30) Palmer, L. C.; Velichko, Y. S.; Olvera de la Cruz, M.; Stupp, S. I. *Philos. Trans. R. Soc. A* **2007**, *365*, 1417–1433.
(31) Peterca, M.; Imam, M. R.; Leowanawat, P.; Rosen, B. M.; Wilson, D. A.; Wilson, C. J.; Zeng, X.; Ungar, G.; Heiney, P. A.; Percec, V. *J. Am. Chem. Soc.* **2010**, *132*, 11288–11305.
(32) Henle, M. L.; Pincus, P. A. *Phys. Rev. E.* **2005**, *71*, 060801.
(33) Chen, T.; Zhang, Z.; Glotzer, S. C. *J. Phys. Chem. C* **2007**, *111*, 4132–4137.
(34) Douglas, J. F.; Dudowicz, J.; Freed, K. F. *Phys. Rev. Lett.* **2009**, *103*, 135701.
(35) Forrey, C.; Muthukumar, M. *J. Chem. Phys.* **2009**, *131*, 105101.
(36) Das, R.; Kiley, P. J.; Segal, M.; Norville, J.; Yu, A. A.; Wang, L.; Trammell, S. A.; Reddick, L. E.; Kumar, R.; Stellacci, F.; Lebedev, N.; Schnur, J.; Bruce, B. D.; Zhang, S.; Baldo, M. *Nano Lett.* **2004**, *4*, 1079–1083.
(37) Balaban, T. S. *Acc. Chem. Res.* **2005**, *38*, 612–623.
(38) Carmeli, I.; Frolov, L.; Carmeli, C.; Richter, S. J. *Am. Chem. Soc.* **2007**, *129*, 12352–12353.
(39) Gnichwitz, J.-F.; Wielopolski, M.; Hartnagel, C.; Hartnagel, U.; Guldi, D. M.; Hirsch, A. *J. Am. Chem. Soc.* **2008**, *130*, 8491–8501.
(40) Gnichwitz, J.-F.; Marczak, R.; Werner, F.; Lang, N.; Jux, N.; Guldi, D. M.; Peukert, W.; Hirsch, A. *J. Am. Chem. Soc.* **2010**, *132*, 17910–17920.
(41) Gröhn, F. *Macromol. Chem. Phys.* **2008**, *209*, 2295–2301.
(42) Gröhn, F.; Klein, K.; Brand, S. *Chem.—Eur. J.* **2008**, *14*, 6866–6869.
(43) Willerich, I.; Gröhn, F. *Chem.—Eur. J.* **2008**, *14*, 9112–9116.
(44) Li, Y.; Yildiz, U. H.; Müllen, K.; Gröhn, F. *Biomacromolecules* **2009**, *10*, 530–540.
(45) Ruthard, C.; Maskos, M.; Kolb, U.; Gröhn, F. *Macromolecules* **2009**, *42*, 830–840.
(46) Reinhold, F.; Kolb, U.; Lieberwirth, I.; Gröhn, F. *Langmuir* **2009**, *25*, 1345–1351.
(47) Yildiz, U. H.; Koynov, K.; Gröhn, F. *Macromol. Chem. Phys.* **2009**, *210*, 1678–1690.
(48) Ruthard, C.; Maskos, M.; Kolb, U.; Gröhn, F. *J. Phys. Chem. B* **2011**, *115*, 5716–5729.
(49) Willerich, I.; Ritter, H.; Gröhn, F. *J. Phys. Chem. B* **2009**, *113*, 3339–3354.
(50) Willerich, I.; Li, Y.; Gröhn, F. *J. Phys. Chem. B* **2010**, *114*, 15466–15476.
(51) Jansen, J. F. G. A.; de Brabander-van den Berg, E. M. M.; Meijer, E. W. *Science* **1994**, *266*, 1226–1229.
(52) Richter-Egger, D. L.; Landry, J. C.; Tesfai, A.; Tucker, S. A. *J. Phys. Chem. B* **2001**, *105*, 6826–6833.
(53) Rainwater, J. C.; Anslyn, E. V. *Chem. Commun.* **2010**, *46*, 2904–2906.
(54) Willerich, I.; Schindler, T.; Ritter, H.; Gröhn, F. *Soft Matter* **2011**, *7*, 5444–5450.
(55) Willerich, I.; Gröhn, F. *Macromolecules* **2011**, *44*, 4452.
(56) Ruthard, C.; Schmidt, M.; Gröhn, F. *Macromol. Rapid Commun.* **2011**, *32*, 706–711.
(57) Willerich, I.; Schindler, T.; Ritter, H.; Gröhn, F. *J. Phys. Chem. B* **2011**, *115*, 9710–9719.
(58) Peng, S.; Wu, C. *Macromolecules* **1999**, *32*, 585–589.
(59) Relative intensities and aggregation numbers but no absolute aggregation numbers were determined from static light scattering because the aggregation behavior in this complex multicomponent system is concentration dependent so that a routine molecular mass distribution is not possible.
(60) "Unchanged" means that when assembly formation is induced by adding HCl, no change in the correlation function can be observed. As depicted in Figure 1a, the relaxation time distribution is not identical to the pure dendrimer as even pure dye solutions can show scattering to some extent even for dyes where no expressed self-aggregation can be observed.
(61) The ζ-potential measurement for the PAMAM dendrimer is not very accurate as its size is too small; however, it can be used as an estimate. Further, the ζ-potential depends on the ratio of particle charge to particle radius. Thus similar values of the ζ-potential can be translated into a similar charge density. This is an effective value realized at the shear plane of the particle in solution.
(62) Kasha, M.; El-Bayoumi, M. A.; Rhodes, J. *J. Chim. Phys.* **1961**, *58*, 916–925.
(63) Moreno-Villoslada, I.; Torres-Gallegos, C.; Araya-Hermosilla, R.; Nishide, H. *J. Phys. Chem. B* **2010**, *114*, 4151–4158.
(64) Moreno-Villoslada, I; Jofre, M.; Miranda, V.; Gonzalez, R.; Sotelo, T.; Hess, S.; Rivas, B. L. *J. Phys. Chem. B* **2006**, *110*, 11809–11812.
(65) Stoesser, P. R.; Gill, S. J. *J. Phys. Chem.* **1967**, *71*, 564–567.
(66) Burrows, S. D.; Doyle, M. L.; Murphy, K. P.; Franklin, S. G.; White, J. R.; Brooks, I.; McNulty, D. E.; Scott, M. O.; Knutson, J. R. *Biochemistry* **1994**, *33*, 12741–12745.
(67) Buurma, N. J.; Haq, I. *J. Mol. Biol.* **2008**, *381*, 607–621.
(68) Wiseman, T.; Williston, S.; Brandts, J. F.; Lin, L. N. *Anal. Biochem.* **1989**, *179*, 131–137.
(69) McGhee, J. D.; von Hippel, P. H. *J. Mol. Biol.* **1974**, *86*, 469–489.
(70) Schwarz, G.; Klose, S.; Balthasar, W. *Eur. J. Biochem.* **1970**, *12*, 454–460.
(71) Handel, T. M.; Cohen, H. L.; Tan, J. S. *Macromolecules* **1985**, *18*, 1200–1206.
(72) Murakami, K. *Langmuir* **2004**, *20*, 8183–8191.
(73) Sinn, C. G.; Dimova, R.; Antonietti, M. *Macromolecules* **2004**, *37*, 3444–3450.

(74) Ikeda, Y.; Beer, M.; Schmidt, M.; Huber, K. *Macromolecules* **1998**, *31*, 728–733.
(75) Lumry, R.; Rajender, S. *Biopolymers* **1970**, *9*, 1125–1227.
(76) Rekharsky, M. V.; Inoue, Y. *Chem. Rev.* **1998**, *98*, 1875–1917.
(77) Grunwald, E.; Steel, C. *J. Am. Chem. Soc.* **1995**, *117*, 5687–5692.
(78) Murakami, K. *Dyes Pigm.* **2002**, *53*, 31–43.
(79) Würthner, F. *Chem. Commun.* **2004**, *40*, 1564–1579.
(80) Schwarz, G. *Eur. J. Biochem.* **1970**, *12*, 442–453.
(81) Schmitz, K. S. *Macroions in Solution and Colloidal Suspension*; Wiley VCH: New York, 1993.
(82) Gröhn, F.; Antonietti, M. *Macromolecules* **2000**, *33*, 5938–5949.
(83) Antonietti, M.; Briel, A.; Gröhn, F. *Macromolecules* **2000**, *33*, 5950–5953.
(84) Van Workum, K.; Jack, F.; Douglas, J. F. *Phys. Rev. E* **2005**, *71*, 031502.
(85) Van Workum, K.; Douglas, J. F. *Phys. Rev. E* **2006**, *73*, 031502.
(86) Sciortino, F.; Tartaglia, P.; Zaccarelli, E. *J. Phys. Chem. B* **2005**, *109*, 21942–21953.
(87) Sayar, M.; Holm, C. *Europhys. Lett.* **2007**, *77*, 16001.
(88) Zollinger, H. *Color Chemistry*, Third ed.; Wiley VCH: Zürich, 2003.
(89) Robinson, C.; Mills, H. A. T. *Proc. R. Soc. London A* **1931**, *131*, 576–595.
(90) Kratky, O.; Pilz, I.; Ledwinka, H. *Mh. Chem.* **1967**, *98*, 227–230.
(91) Clarke, H. T. *J. Org. Chem.* **1971**, *36*, 3816–3819.
(92) Ohsawa, K.; Muruta, M.; Oshima, H. *Colloid Polym. Sci.* **1986**, *264*, 1005.
(93) Hunter, R. J. *Foundations of Colloid Science*; Oxford University Press: New York, 2001.